The Use of Ultrasound to Mitigate Membrane Fouling in Desalination and Water Treatment

Muhammad Qasim [a], Noora N. Darwish [a], Sahar Mhiyo [b], Naif A. Darwish [a*], Nidal Hilal [c]

[a]*Department of Chemical Engineering, American University of Sharjah, P.O. Box 26666, Sharjah, United Arab Emirates*

[b]*Faculty of Chemical and Petroleum Engineering, Al Baath University, Homs PO Box 77, Syria*

[c]*Centre for Water Advanced Technologies and Environmental Research (CWATER), College of Engineering, Swansea University, Fabian Way, Swansea SA1 8EN, UK.*

Abstract

Fouling is recognized as a serious challenge in reverse osmosis desalination and in different membrane-based separation technologies. Membrane fouling not only reduces the permeate flux and the membrane productivity but also significantly decreases the membrane lifespan, increases the energy and feed pressure requirement, and increases membrane maintenance and replacement costs. As a result, the consequences of membrane fouling have always stimulated research investigations into different fouling mitigation strategies. In this context, application of ultrasound is an effective technique that can be used as an external aid for both membrane fouling control and membrane cleaning. The purpose of this review paper is to provide an updated and comprehensive review of ultrasound as an effective tool for membrane flux enhancement and membrane cleaning. In addition to briefly discussing the mechanisms of membrane fouling, theories related to ultrasonic waves, acoustic cavitation, cavitational collapse, and ultrasound-induced effects are addressed. The key challenges in industrial application of ultrasound for flux enhancement and membrane cleaning are also discussed.

Keywords: Membrane fouling, membrane cleaning, flux enhancement, ultrasound, pretreatment

Highlights

- An updated review of ultrasound-assisted membrane fouling mitigation is provided
- Mechanisms of membrane fouling are briefly addressed
- Theoretical aspects of ultrasound are discussed
- Application of ultrasound for flux enhancement and membrane cleaning are reviewed
- Challenges of ultrasound application in membrane-based processes are discussed

1. Introduction

Membranes are of immense importance in industrial separation processes and are extensively used in a wide range of applications including desalination [1–6], wastewater treatment [7–12], food and beverage processing [13–17], biotechnology [18–20], and petrochemical processing [21,22]. Membrane-based separation processes are typically characterized by advantages such as selective separation, low space requirement, process and plant compactness, low chemical requirement, operational simplicity, and ease of process automation [23,24]. Despite these advantages, permeate flux decline is one of the main limitations in membrane-based technologies. The flux decline is mainly attributed to the concentration polarization and membrane fouling phenomena [25]. Concentration polarization occurs due to solute build-up in the mass transfer boundary layer near the membrane rejection surface and results in decreased effective transmembrane pressure (TMP) owing to the generation of osmotic back pressure [26,27]. On the other hand, membrane fouling is a complex phenomenon that involves deposition of materials on the membrane surface or within the membrane pores [28]. While concentration polarization is essentially reversible [29], membrane fouling presents a greater challenge and contributes significantly to the decline in flux, productivity, and membrane lifespan, increase in the energy consumption due to high feed pressure requirement, and increase in the membrane maintenance, cleaning, and replacement costs [23]. Therefore, research investigations into fouling control and membrane cleaning methods are of considerable importance.

Fouling control methods aim to decrease the likelihood of membrane fouling. Often pretreatment methods are used as preventative measures for controlling membrane fouling. These include the use of prefilters, screens, precipitation, coagulation, flocculation, or chemicals to reduce the amount of foulants in the feed [30–33]. In addition, membrane surface modification may be performed to lower the affinity of foulants for the membrane surface [30,34–39]. Membrane fouling can also be controlled by optimizing the operating conditions such as pH, temperature, pressure, and hydrodynamics [30,34]. Other methods to control membrane fouling rely on enhancing the shear on the membrane surface. These methods include gas bubbling, rotating disks/rotors, rotating membranes, and vibratory systems [30,40,41]. Despite being effective, scale-up and equipment cost are major challenges in industrialization of the shear-enhanced fouling control methods [41].

Membrane cleaning methods are typically used when fouling control methods fail and the membrane must be cleaned for full or partial removal of the foulants. Cleaning methods may be classified into chemical or physical methods. Chemical cleaning methods involve application of

chemical agents such as caustic soda, oxidants, acids, chelates, or proprietary surfactants in order to weaken cohesion forces between the foulants and the membrane surface [42]. These methods usually require large amount of chemicals, pose safety concerns, cause damage to the membrane, and generate waste streams that result in secondary pollution [30]. Physical cleaning methods, on the other hand, involve application of hydraulic or mechanical cleaning forces in order to loosen and detach the foulants [43]. This may include cleaning the membrane using a hose pipe, sponge, or brush that requires significant physical effort [27]. Backwash has proved to be an effective physical cleaning method. However, it is only applicable to tubular and hollow fiber membranes due to high pressure durability requirement [30,44]. In addition, hydraulic flushing (forward and reverse) can be used that involves removal of surface deposits using a rinsing solution. However, flushing method is typically employed after the foulants have been loosened by other cleaning method such as chemical cleaning and backwash [43]. Also, both flushing and backwash require periodic process shutdown.

Ultrasound application provides an alternative technique for membrane fouling control and membrane cleaning in desalination and water treatment. Although there are numerous experimental studies on the use of ultrasound in different membrane-based technologies, only few technical reviews exist in the literature [27,30,45]. This review paper outlines the theory and mechanisms of membrane fouling and ultrasound irradiation and aims to provide an updated and comprehensive review of ultrasound-assisted membrane fouling mitigation. The key challenges related to ultrasound application in membrane processes are also discussed.

2. Theory and mechanisms of membrane fouling

Membrane fouling is a challenge in both pressure-driven membrane processes such as microfiltration (MF), ultrafiltration (UF), nanofiltration (NF), and reverse osmosis (RO) and osmotically-driven membrane processes such as forward osmosis (FO) and pressure-retarded osmosis (PRO). Fouling is also inevitable in other membrane-based processes including membrane bioreactor (MBR) and membrane distillation (MD). An understanding of membrane fouling fundamentals and the involved mechanisms is crucial to the development of novel approaches for fouling control and membrane cleaning. Therefore, this section outlines the fundamental concepts in membrane fouling.

Membrane fouling is a complex phenomenon that involves physical and chemical interactions between the different foulants present in the feed and between the foulants and the membrane surface. The overall effect of fouling is to decrease the active membrane area or increase the

resistance across the membrane leading to a decreased flux for a given TMP. In general, membrane fouling may occur in the form of adsorption, pore blockage, particle deposition, or gel formation [28]. Adsorption refers to specific interactions between the foulants and the membrane surface or the membrane pore walls that result in an increased hydraulic resistance. Pore blockage, on the other hand, involves plugging of the membrane pores that results in a decreased flux across the membrane. Deposition of foulants simply refers to the layer by layer accumulation of foulants on the membrane surface that offers an additional hydraulic resistance known as cake resistance. In case of fouling due to gel formation, cross-linked three-dimensional networks of deposited particles, such as macromolecules and colloidal substances, are formed on the membrane surface. The gel layers lack of connectivity between the pores and, therefore, present high resistance for mass transport across the membrane [46]. Accumulation of foulants on the surface is often termed as external fouling while fouling within the membrane pores is also known as internal fouling.

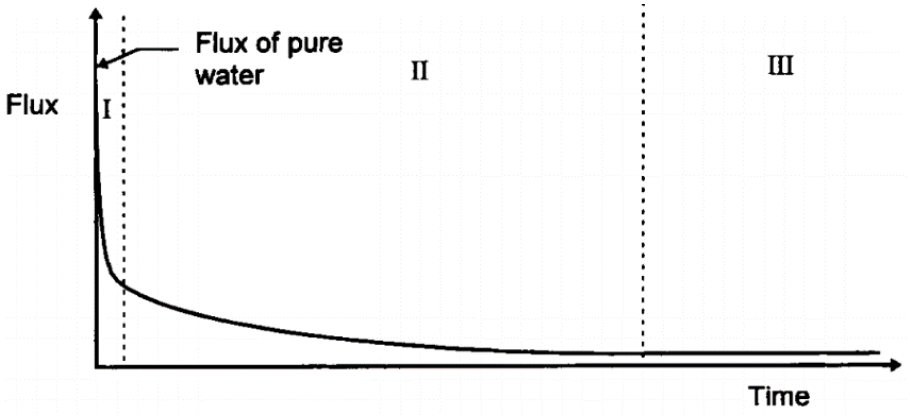

Fig. 1. The three stages of flux decline due to membrane fouling. Stage I: quick initial decline, stage II: long-term steady decline in flux, stage III: time-independent steady-state flux (adopted from [47])

The typical flux-time curve depicted in Fig. 1 [47] highlights the serious consequences of membrane fouling in UF and MF processes. Typically, the flux decline occurs in three stages. In stage I, there is a quick flux decline due to rapid pore blocking at the start-up of the process. In stage II, the flux further declines which is attributed to the formation and growth of the cake layer. The flux continues to decline in this stage as the cake layer grows and becomes thicker. In stage III, the process reaches steady-state and the cake grows to its equilibrium thickness [47]. The difference between the initial pure water flux and the steady-state flux can be very large. For instance, in UF and MF, the steady-state flux obtained is usually less than 5% of the pure water flux [28].

Different types of foulants may be encountered in membrane-based separation processes depending on the characteristics of the feed water. Generally, the foulants are classified into the following four types [23]:

- Organic foulants: These consist of dissolved or colloidal organic matters that are deposited/adsorbed on the membrane and include humic acid, fulvic acid, peptides, proteins, polysaccharides, and many others
- Inorganic foulants: These include dissolved or sparingly soluble inorganic components that precipitate due to pH changes or due to oxidation. Examples include calcium sulfate, calcium carbonate, silica, iron, manganese, etc.
- Particulates/colloids: These include organic and inorganic particles or colloids that accumulate on the membrane surface, block the pores, or form cake layer, for example, suspended solids, silt, and clay
- Microbiological organisms: These cause biofouling by adhesion and growth of bacterial and fungal species and excretion of extracellular materials

Membrane fouling is affected by a number of factors such as material, type, pore size distribution, and surface characteristics of the membrane, feed solution chemistry, and hydrodynamics of the membrane process [28].

2.1. Organic fouling

Organic fouling is typical in membrane-based separation processes due to the ubiquitous presence of dissolved organic matter (DOM) in surface water, wastewater, and sewage. DOM can be categorized into: (1) natural organic matter (NOM) that are produced through metabolic reactions in drinking water sources, (2) synthetic organic compounds (SOC) that are discharged into wastewater streams from household and industries, and (3) soluble microbial products (SMP) that are formed during biological water treatment [23]. In case of NOM, the major constituents in surface or ground waters are humic substances (humic acids, fulvic acids, and humin) formed by decomposition of plant and animal residues [48]. Humic substances contain both aromatic and aliphatic components of carboxylic and phenolic functional groups. Also, NOM constitutes non-humic fractions that are composed of transphilic acids, amino acids, proteins, and carbohydrates [49]. NOM can cause organic fouling in several ways. It can deposit or adsorb within the membrane pores, form a gel layer on the membrane surface, or bind other particles to form NOM/particle fouling layer on the membrane surface [50]. In addition, organic fouling may be caused by transparent exopolymer particles (TEPs) primarily formed from polysaccharides

excreted by microalgae [51]. Also, effluent organic matter (EfOM), composed of NOM and SMP, from biological wastewater treatment can cause organic fouling of membranes. EfOM may contain compounds such as polysaccharides, proteins, enzymes, nucleic acids, antibiotics, and steroids [23]. Organic fouling, in general, is a complex phenomenon that is significantly affected by the feed water chemistry, foulant-membrane surface interactions, and foulant-foulant interactions [52]. Adsorption is considered to be the key mechanism in the initial buildup of organic fouling layer. Also, the molecular size and the hydrophilicity or hydrophobicity of NOM play a key role in the organic fouling of membranes and the resulting flux decline [53].

2.2. Inorganic fouling

Inorganic membrane fouling is often termed as 'mineral scaling'. It is caused by the presence of high concentrations of inorganic compounds in the feed water. Some common examples of inorganic foulants with low solubility include calcium sulfate ($CaSO_4$), calcium carbonate ($CaCO_3$), barium sulfate ($BaSO_4$), and silica (SiO_2). The main cationic species that account for inorganic fouling include Ca^{+2}, Mg^{+2}, Fe^{+3}, and Al^{+3}. On the other hand, the main inorganic species that are in equilibrium with potential scaling components typically include OH^-, F^-, CO_3^{-2}, SO_4^{-2}, orthophosphate, and silicic acids [23]. Inorganic fouling or scale formation on the membrane surface is governed by both crystallization and transport mechanisms. Crystallization occurs as a result of ion precipitation on the membrane surface. This happens when the activity of ions in the feed water is above the saturation limit, that is, the feed is supersaturated. Scaling due to crystallization occurs by two possible pathways: bulk (homogeneous) crystallization and surface (heterogeneous) crystallization. In bulk crystallization, crystal particles deposit on the membrane surface and form a cake layer after being formed in the bulk phase through homogeneous crystallization. Supersaturated solutes allow for agglomeration of scale-forming ions due to random collisions in the bulk phase. The cluster of ions coalesces and results in precipitation after growing above a critical size. In case of surface crystallization, crystals are directly formed on the membrane surface and scale formation takes place through lateral growth of crystals [54,55]. Fig. 2 depicts the bulk and surface crystallization phenomena.

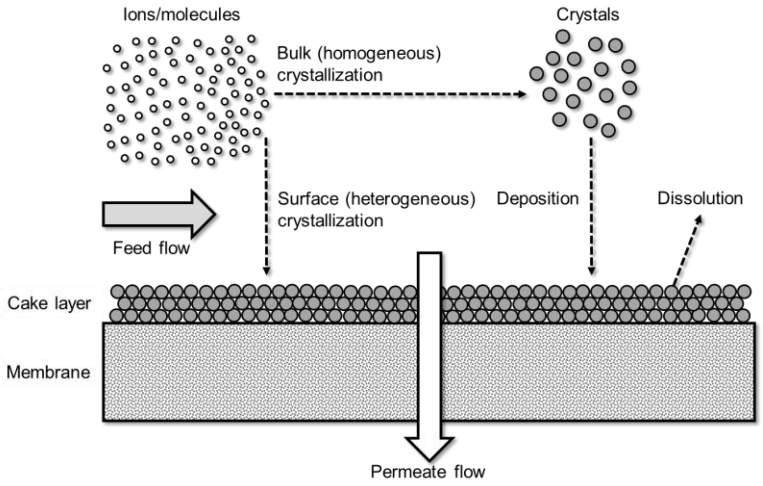

Fig. 2. Mechanism of bulk and surface crystallization (modified after [54])

Inorganic fouling is affected by a number of factors such as membrane surface roughness, the region and degree of supersaturation, shear across the membrane, TMP, and the feed solution chemistry [54]. Membranes with rough surfaces are more prone to inorganic fouling than those with smooth surfaces. This is because higher surface roughness increases the surface free energy which consequently increases the adhesiveness of the membrane. Inorganic fouling also tends to increase at high degrees of supersaturation, low shear rates, and high TMP. Also, inorganic fouling is more severe with feed water containing particles of smaller sizes and higher concentrations.

2.3. Colloidal Fouling

Based on their size, particulate or colloidal matter is typically classified into: (1) settleable solids (> 100 μm), (2) supra-colloidal solids (1 μm to 100 μm), (3) colloidal solids (10 Å to 1 μm), and (4) dissolved solids (< 10 Å) [23,56]. Typical examples of inorganic colloids include silt, aluminum silicate clays, colloidal silica, elemental sulfur, precipitated iron, and corrosion products [23]. Organic colloids, on the other hand, include proteins, carbohydrates, fats, oils and greases [57,58]. In membrane processes, permeate flux is the main mechanism for the transport of colloidal particulates from the bulk feed to the membrane surface. At the same time, cross flow induces reverse transport of colloids from the membrane surface to the bulk feed. This reverse transport is usually governed by Brownian diffusion, shear-induced diffusion, turbulent transport, particle rolling, inertial-lift forces, and particle-particle interaction forces [59].

In case of non-porous membranes, such as RO and NF membranes, colloidal fouling is caused by accumulation of particles on the membrane surface resulting in cake layer formation. This

results in an increased hydraulic resistance and a corresponding decline in the transmembrane flux. In case of porous membranes, such as MF and UF membranes, the pore size is large enough to allow for pore plugging. Therefore, colloidal fouling is caused by both pore plugging and surface accumulation [54].

It has been reported that only very small colloidal matter is of major concern in membrane fouling since colloids with size greater than 0.45 μm can be easily removed by backwashing [23,60]. The physiochemical properties and surface charge of colloids significantly depends on the feed solution chemistry such as pH, ionic strength, and ionic composition [58]. Therefore, feed solution chemistry is an important factor in colloidal fouling. In addition, colloidal fouling also depends on membrane properties. Smooth and more hydrophilic membranes with low surface charge tend to exhibit better colloidal fouling resistance at the initial fouling stage [58,61–63]. Also, colloidal fouling depends on the hydrodynamic conditions with fouling being more severe at high flux and low cross-flow velocity [58].

2.4. Biofouling

Biofouling is a consequence of the deposition, growth, and metabolism of microbiological cells (bacteria, algae, protozoa, and fungi) or flocs and the development of biofilm on the membrane. Biofouling is considered as a contributing factor to more than 45% of all membrane fouling [64] and, therefore, represents a serious operational problem in membrane-based processes.

Biofouling is initiated through attachment of microbiological cells to the membrane surface that leads to biofilm formation. After attachment, the microbiological cells multiply and grow at the expense of feed nutrients and/or the organics adsorbed on the membrane surface. At the same time, extracellular polymeric substances (EPS) are excreted that anchor the microbiological cells and allow for further colonization on the membrane surface. After growth, the cells detach and disperse to the new sites on the membrane surface in order to reinitialize the biofilm formation [65]. Fig. 3 depicts the biofilm formation on a solid surface.

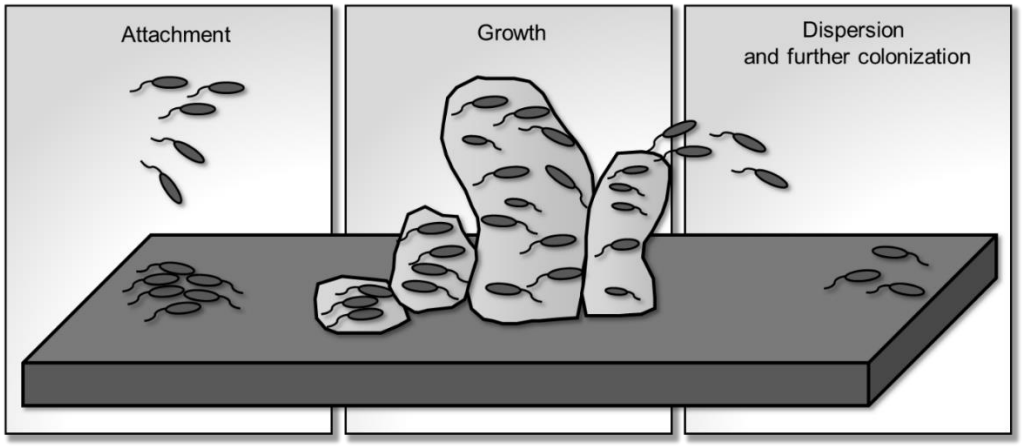

Fig. 3. Biofilm formation on solid surface (modified after [65])

The formation of biofilm is stepwise and includes: (a) formation of a conditioning film by absorption of organic species (macromolecules, proteins, etc.) on the membrane surface, (b) transport of microbiological cells from the bulk feed to the conditioning film, (c) attachment of cells to the membrane surface, and (d) formation of biofilm by cell growth [66]. The attachment of cells is affected by the membrane properties such as material, roughness, hydrophobicity, and surface charge. In addition, the characteristics of the microbiological cells and the feed water also affect the attachment of cells to the membrane surface [23,66].

EPS play a significant role in biofouling. These substances are usually high molecular weight secretions of the microbiological cells such as polysaccharides, proteins, nucleic acids, and lipids. EPS can be classified into bound EPS and soluble EPS (or SMP). Bound EPS are strongly bound to the microbiological cells while soluble EPS are loosely bound and occur mainly as dissolved substances in the bulk feed. EPS contain both hydrophilic and hydrophobic functional groups which allows for their deposition on both hydrophilic and hydrophobic membranes. EPS provide a means of binding the cells together in the form of three-dimensional matrices. In addition, EPS affect the structural stability of the biofilms and the stability, adhesion ability, and the surface characteristics of the microbiological cells [66].

3. Theoretical aspects of ultrasound

3.1. Ultrasound phenomenon

Ultrasound, also known as ultrasonic wave, or ultrasonic sound, is a sound (acoustic) wave traveling at a frequency higher than 20 kHz that is above the normal human hearing range [67]. In comparison with the audible sound, ultrasound is characterized by the ability to generate

special physical and chemical effects by transmitting high mechanical power via small mechanical movements [45,68]. Fig. 4 shows a typical ultrasonic wave whose key parameters are defined in Table 1.

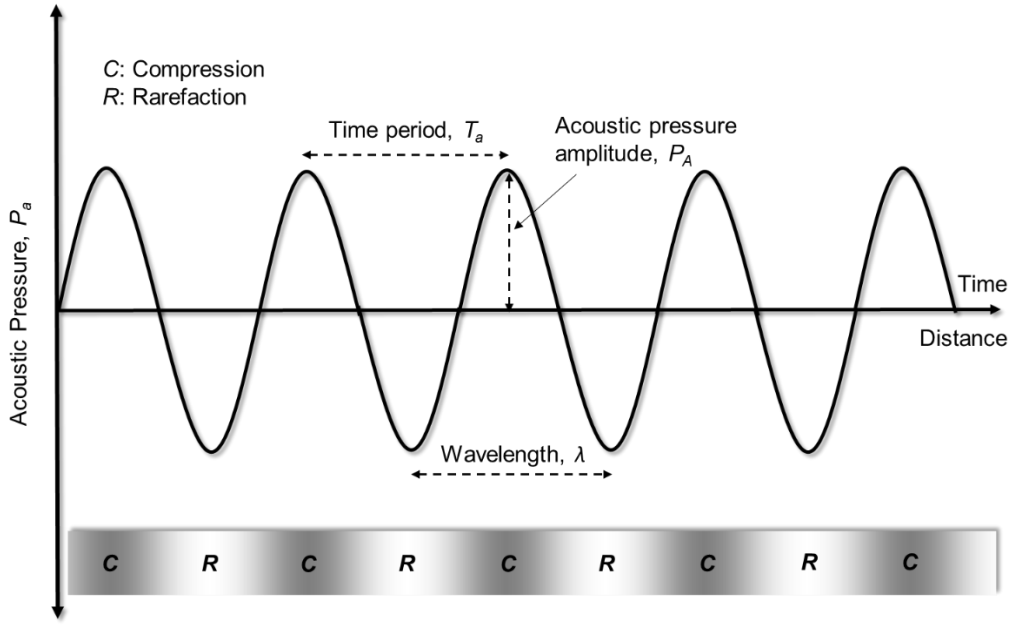

Fig. 4. Schematic diagram of an ultrasonic wave consisting of a series of compression and rarefaction waves (propagation is from left to right)

As depicted in Fig. 4, ultrasound propagates through a fluid by a series of compression and rarefaction (expansion) waves. As a consequence of such propagation, the molecules in the fluid are subjected to compression and rarefaction cycles parallel to the direction of wave propagation. This creates an acoustic pressure (P_a) in addition to the hydrostatic pressure (P_0) of the fluid. The acoustic pressure created is given by the following equation [25]:

$$P_a = P_A \sin(2\pi f t) \quad (1)$$

Where, P_A, f, and t represent the acoustic pressure amplitude, frequency, and time, respectively.

Table 1

Definitions of ultrasonic wave parameters [68]

Parameter (Symbol, unit)	Definition
Wavelength (λ, m)	Length for one pressure oscillation
Time period (T_a, s)	Time for one pressure oscillation
Frequency (f, Hz)	Number of pressure oscillations per unit time ($f = 1/T_a$)
Ultrasound power (P, W)	Time rate of ultrasonic energy passing through a surface perpendicular to the direction of propagation
Ultrasound speed (c, m/s)	Distance of propagation per unit time ($c = f\lambda$)
Ultrasound intensity (I, W/m^2)	Ultrasonic energy passing a unit surface perpendicular to the direction of propagation per unit time
Acoustic pressure amplitude (P_A, Pa)	Maximum height of the ultrasonic wave
Acoustic pressure (P_a, Pa)	Pressure created as a result of compression or rarefaction zones relative to the fluid hydrostatic pressure

Based on the frequency, three distinct categories of ultrasound can be defined, namely power ultrasound (20 kHz – 100 kHz), high frequency ultrasound (100 kHz – 1 MHz), and diagnostic ultrasound (1 MHz – 500 MHz) [69]. However, for cleaning and processing applications in the industry, ultrasound with frequency covering the whole range between 20 kHz – 500 kHz is widely used [25].

3.2. Acoustic cavitation

During the compression cycle, the molecules in the fluid are subjected to a positive acoustic pressure that drives the molecules close to one another. On the other hand, during the rarefaction cycle, a negative pressure is exerted that pulls the molecules apart. If the pressure amplitude and the resulting tensile stress during rarefaction exceeds the tensile strength of the liquid, the intermolecular forces are unable to hold the molecules together and small vapor-filled voids or cavitation bubbles are formed within the liquid [69]. This phenomenon is known as acoustic cavitation. The minimum acoustic pressure required to overcome the liquid tensile strength and form a cavitation bubble of initial radius R_0 is called the Blake threshold (P_b) and is given by the following equation [68,70]:

$$P_b = P_0 + \frac{2}{3}\sqrt{\frac{(2\sigma/R_0)^3}{3(P_0 + 2\sigma/R_0)}} \quad (2)$$

Where, P_0 is the hydrostatic pressure on the liquid and σ is the surface tension of the liquid. In Eq. (2), the term $(2\sigma/R_0)$ represents the surface tension of the cavitation bubble. Also, Eq. (2) neglects the vapor pressure and inertial and viscous effects [70].

The formation of cavitation bubbles in a liquid is generally attributed to the nucleation phenomenon and the presence of weak spots such as free-floating gas bubbles, solids impurities, dissolved solids, and gas pockets in the crevices of the solids that act as nuclei [71–73]. Typically, ultrasound is unable to produce cavitation bubbles in pure liquids that naturally possess very high tensile strengths. However, the presence of impurities significantly reduces the liquid tensile strength and the required Blake threshold to initiate cavitation. For instance, the Blake threshold for impure liquids is approximately 1-10% of the Blake threshold for pure liquids [68,74].

3.3. Cavitation bubble growth

Once the cavitation bubbles are formed, they may dissipate back into the liquid or grow in size. The growth of cavitation bubbles occurs due to the coalescence and rectified diffusion phenomena [72]. Coalescence simply refers to the process where small cavitation bubble combine to form larger bubbles. Rectified diffusion, on the other hand, refers to the bubble growth under the repeated compression and rarefaction cycles generated by the ultrasound. During the compression cycle, the bubbles are compressed and the contained material (liquid vapors and gases) is released into the liquid. The amount of material entering or leaving is proportional to the surface area of the bubbles. Overall, the amount of material expelled is smaller than the amount taken in during the rarefaction cycle due to smaller surface area available during the compression cycle. This known as the area effect. As a result of the area effect, the bubbles continuously grow in size in the presence of the ultrasonic field.

In addition to the area effect, shell effect is also an important consideration in rectified diffusion [75]. Shell effect is related to the thickness of the liquid shell around the cavitation bubbles. During the compression cycle, the bubbles shrink while the thickness of the liquid shell around them increases. This decreases the gas concentration near the wall of the bubbles. Therefore, a small concentration gradient is available for gas movement out the bubbles covered with thick liquid shells. During the rarefaction cycle, the bubbles expand and the thickness of the liquid shell decreases. This leads to an increase in gas concentration near the wall of the bubbles. For each

bubble under rarefaction, a large concentration gradient is available along with a thin liquid shell. In comparison with the compression cycle, larger amount of gas moves into the bubbles during the rarefaction cycle. Therefore, the net effect is to increase the size of the bubbles [76]. Typically, the bubbles grow to a maximum size of 2-150 μm [68].

3.4. Cavitational collapse

After growing, degassing may occur where the bubbles may leave the liquid due to buoyancy. In case the bubbles grow to a critical size (known as resonance size, R_r) by rectified diffusion, they may fluctuate around this size, or grow to a size at which they collapse [77]. The resonance size (R_r) of the bubble is a function of ultrasound frequency and can be estimated using the following equation [72]:

$$R_r = \sqrt{\frac{3\gamma P_0}{\rho\omega^2}} \tag{3}$$

Where, ω is the angular frequency of the ultrasound, γ is the specific heat ratio of the gas in the bubble, and ρ is the liquid density. In case of air bubbles in water, the following simplified equation can be used to estimate the resonance radius [72]:

$$R_r \approx \frac{3}{f} \tag{4}$$

Where f is the ultrasound (acoustic) frequency. The collapse of the bubbles (also known as cavitational collapse) is governed by the bubble oscillation frequency (f_b) given by the following equation [68]:

$$f_b = \frac{1}{2\pi R}\sqrt{\frac{3\gamma}{\rho}\left(P_0 + \frac{2\sigma}{R}\right)} \tag{5}$$

Where, R is the bubble radius. If the resonant frequency is less than the ultrasound frequency at the end of the compression cycle, the bubbles will remain intact and continue the growth cycle. This is called non-inertial, steady, or stable cavitation where the bubbles oscillate over many compression and rarefaction cycles until they collapse. However, if the resonant frequency becomes equal to or greater than the ultrasound frequency, the bubbles will grow rapidly and then collapse violently into smaller bubbles within a single acoustic cycle [25,68]. This is known as transient or inertial cavitation where the lifetime of the bubbles is very short. Stable cavitation

typically occurs at low intensities of the ultrasound whereas transient cavitation occurs at high intensities. However, it is important to note that this classification of cavitation is ambiguous since stable cavitation can lead to transient cavitation and transient cavitation can produce smaller bubbles that undergo stable cavitation [69]. Figure 5 summarizes the cavitation bubble growth and the cavitational collapse in an ultrasonic field.

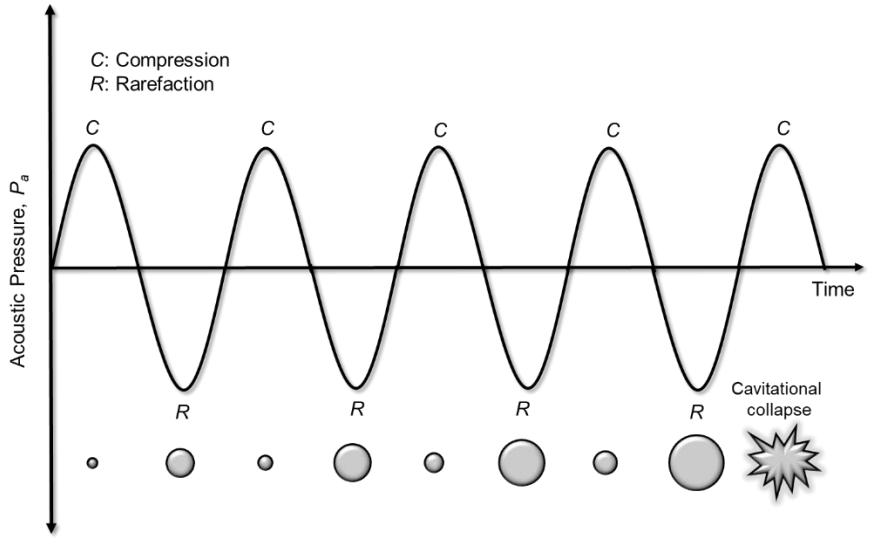

Fig. 5. Schematic diagram of acoustic cavitation, bubble growth, and cavitational collapse

3.5. Dynamics of bubble growth

The radial growth of a single stable bubble is governed by the Rayleigh-Plesset equation given below [68,78]:

$$R\frac{d^2R}{dt^2}+\frac{3}{2}\left(\frac{dR}{dt}\right)^2=\frac{1}{\rho}\left[\left(P_0+\frac{2\sigma}{R_0}\right)\left(\frac{R_0}{R}\right)^{3\gamma}-\frac{2\sigma}{R}-\frac{4\mu}{R}\left(\frac{dR}{dt}\right)-P_\infty\right] \quad (6)$$

Where, R is the radius of the growing bubble, μ represents the liquid viscosity, and P_0 and P_∞ represent the pressure near the bubble and at infinite distance from the bubble, respectively. Eq. (6) assumes that the liquid is incompressible and the bubble is filled with an ideal gas and behaves as an adiabatic system. The pressure at infinite distance from the bubble (P_∞) depends on time (t) and is given as follows [78]:

$$P_\infty = P_0 - P_A \sin(\omega t) \quad (7)$$

In case of radial growth of a gas-filled transient bubble, the following equation is applicable [78]:

$$R\frac{d^2R}{dt^2}+\frac{3}{2}\left(\frac{dR}{dt}\right)^2=\frac{1}{\rho}\left[P\left(\frac{R_{max}}{R}\right)^{3\gamma}-P_m\right] \quad (8)$$

Where, R_{max} is the maximum bubble radius before collapse, P is the pressure (sum of vapor pressure, P_v and gas pressure, P_g) inside the bubble at the maximum radius ($P = P_v + P_g$), and P_m is the liquid pressure at the moment of transient collapse ($P_m = P_0 + P_A$). The bubble collapse time (τ_m) can be estimated using the following equation [78]:

$$\tau_m=0.915R_{max}\left(1+\frac{P}{P_m}\right)\sqrt{\frac{\rho}{P_m}} \quad (9)$$

3.6. Effects of cavitational collapse

Cavitational collapse is characterized by the emission of short bursts of light, a phenomenon known as sonoluminescence [72]. In addition, the violent collapse of transient cavitation bubbles can produce important mechanical and chemical effects in liquid systems. The cavitation bubbles basically provide a means of concentrating the ultrasonic energy. Therefore, upon violent collapse, the cavitation bubbles act as hotspots and generate very high local temperatures and pressures. Typically, the temperatures and pressures can reach up to 5000 K and 1000 atm, respectively [77,79]. In addition, the lifetime of these hotspots is very short leading to very high heating and cooling rates, typically exceeding 10^9 Ks^{-1} [79]. Assuming ideal gas inside the bubbles and that the surface tension and viscosity of the fluid are neglected, the maximum temperature (T_{max}) and the maximum pressure (P_{max}) inside a collapsing bubble can be estimated using the following equations [70,78]:

$$T_{max}=T_0\left[\frac{P_m}{P}(\gamma-1)\right] \quad (10)$$

$$P_{max}=P\left[\frac{P_m}{P}(\gamma-1)\right]^{\gamma/(\gamma-1)} \quad (11)$$

Where, T_0 is the ambient (experimental) temperature.

The extreme temperature and pressure conditions also provide sites for high-energy sonochemical reactions. These reactions are typically explained on the basis of the “hot spot”

model. According to this model, there are three regions (shown in Fig. 6) for the occurrence of sonochemical reactions: (1) a hot gaseous nucleus (thermolytic center), (2) a interfacial region, and (3) the bulk liquid at ambient temperature [79,80]. Within these regions, sonochemical reactions involving free radicals can take place during the cavitational collapse.

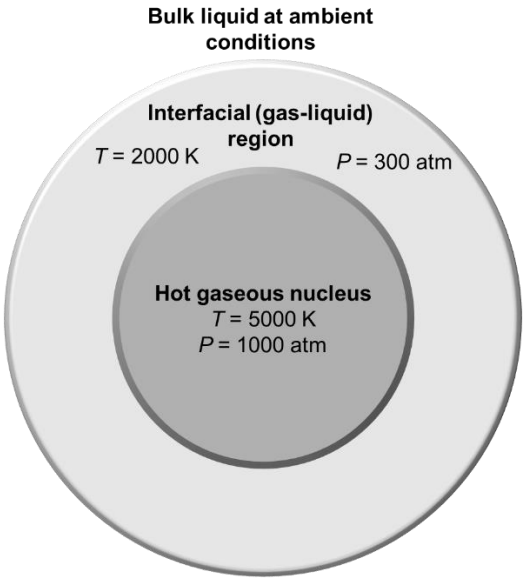

Fig. 6. Zones for sonochemical reactions (modified after [79])

High temperature and pressure conditions in the gaseous nucleus break the bonds of water, vapors, and other constituent gases present within the bubble resulting in the formation of radical or excited chemical species. Water molecules, if present, dissociate to form $H^{\bullet}$ and $OH^{\bullet}$ radicals. Similarly, if present, nitrogen dissociates to create $N^{\bullet}$ radicals. The produced radicals either react to form new molecules or radicals or diffuse into the interfacial region and the bulk liquid. A complete list of reactions and their mechanisms can be found elsewhere [80].

The temperature and pressure in the interfacial region, involving the liquid shell around the collapsing bubble, is about 2000 K and 300 atm, respectively [79]. This region involves combustion and free radical reactions. Within the bulk liquid, there is insignificant primary sonochemical activity. However, small amount of free radicals from the nucleus and the interfacial region may move into the bulk liquid to cause some secondary reactions [79].

3.7. Factors affecting acoustic cavitation and cavitational collapse

Several factors affect the acoustic cavitation phenomenon and the resulting collapse of the cavitation bubbles in an ultrasonic field. These factors are briefly discussed below:

3.7.1. Ultrasonic frequency

Low frequency of ultrasound increases the size of the produced cavitation bubbles and hence, leads to more violent cavitational collapse [25]. At high ultrasound frequencies, acoustic cavitation and cavitational collapse both decrease owing to two main reasons. First, the negative acoustic pressure during the rarefaction cycle becomes insufficient to initiate cavitation. Second, the compression cycle becomes fast and does not allow for sufficient time for the bubbles to collapse [69,78].

3.7.2. Ultrasound intensity

Acoustic cavitation exhibits an optimum with respect to the ultrasound intensity. The power intensity can be determined calorimetrically or from the input or output power per unit area of the ultrasound transducer [45]. By the definition given in Eq. 12 below, ultrasound intensity (I) is directly proportional to the acoustic pressure amplitude (P_A):

$$I = \frac{P_A^2}{2\rho c} \tag{12}$$

Where, c is the speed of the ultrasonic wave. An increase in the intensity increases the acoustic pressure amplitude. This decreases the collapse time (τ_m) based on Eq. (9). Also, increasing the acoustic pressure amplitude increases the maximum temperature (T_{max}) and the maximum pressure (P_{max}) upon bubble collapse based on Eq. (10) and (11), respectively. As a result, the collapse tends to be more rapid and violent at high ultrasound intensity. However, the ultrasound intensity cannot be increased beyond a certain critical value. This is because at very high acoustic pressure amplitudes, the bubbles become very large and the time available for collapse during the compression cycle tends to be insufficient [70]. In addition, the large number of bubbles created at high intensity may cause dampening effect and reduce the effectiveness of the ultrasound [25].

3.7.3. External pressure

According to Eq. (9), an increase in the external static pressure (P_0) decreases the collapse time. Also, as per Eq. (10) and (11), increasing the external pressure increases T_{max} and P_{max} upon bubble collapse. Therefore, increasing the external pressure will lead to more rapid and violent cavitational collapse. However, high external pressure also decreases the liquid vapor pressure. This will lead to an increase in the ultrasound intensity required to initiate cavitation [69].

3.7.4. Bulk liquid temperature

Acoustic cavitation also exhibits an optimum with respect to the liquid temperature. Increasing the temperature results in an increase in the liquid vapor pressure (P_v). Therefore, the cavitational collapse becomes less violent due to decrease in T_{max} and P_{max} based on Eq. (10) and (11), respectively. However, for most liquids, increasing the temperature also decreases the viscosity which favors acoustic cavitation. Viscous liquids, being sluggish, do not allow for easy formation of cavitation bubbles [25,70].

3.7.5. Liquid characteristics

Cavitation bubbles tend to form readily in liquids with low viscosity, low surface tension, and high vapor pressure [69]. However, high vapor pressure also results in less violent bubble collapse (as explained in Section 2.7.4). Also, the presence of high concentration of solid particles decreases the acoustic cavitation phenomenon due to scattering and weakening of ultrasonic waves [25,68].

3.7.6. Gas characteristics

According to Eqs. (10) and (11), the intensity of cavitational collapse depends on the specific heat ratio of the gas inside the bubble (γ). Also, increasing the amount of dissolved gases increases the number of nuclei available for the formation of cavitation bubbles. However, at the same time, the gas pressure inside the bubble (P_g) increases which results in less violent cavitational collapse due to decrease in T_{max} and P_{max} (Eqs. (9) and (10)). In addition, gases with low thermal conductivity create more local heating during bubble collapse [68].

4. Ultrasound effects relevant to membrane fouling

Ultrasound has the ability to produce important physical phenomena in heterogeneous solid-liquid systems which may release the particles from a fouled membrane. These physical phenomena include: acoustic streaming, microstreaming, and the generation of microstreamers, microjets, and shock waves.

Acoustic streaming is a form of fluid flow that results from the absorption of acoustic (ultrasonic) energy and does not require cavitational collapse [77]. As the ultrasonic waves propagate, the wave momentum is absorbed by the liquid due to its finite viscosity. As a result, unidirectional flow currents are created within the liquid [73]. Acoustic streaming generates low flow velocity (about 10 ms^{-1}) and occurs over up to a distance of only few centimeters from the ultrasonic transducer [77]. The flow velocity increases at higher values of ultrasound frequency and power intensity. In

the vicinity of a solid surface, such as a fouled membrane, the liquid flow created by acoustic streaming is obstructed resulting in unidirectional flow currents parallel to the solid surface which may detach the foulants. A schematic representation of acoustic streaming is shown in Fig. 7.

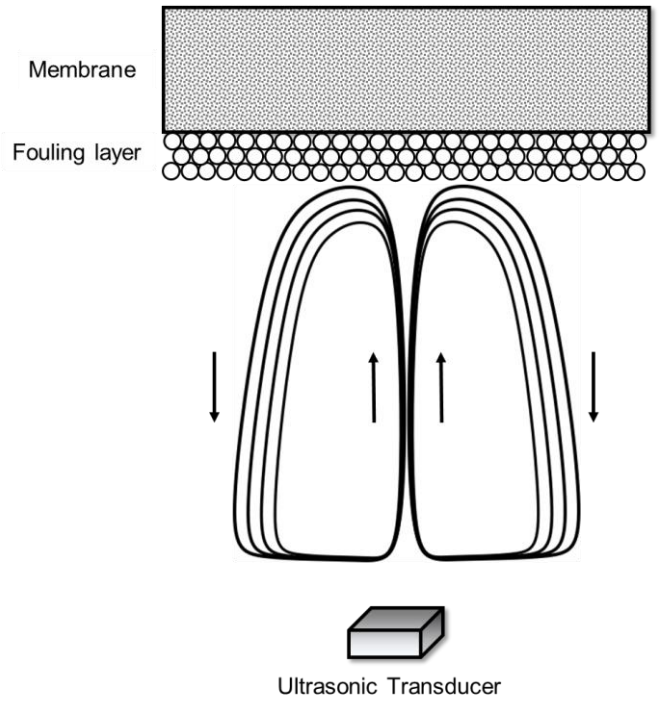

Fig. 7. Schematic representation of acoustic streaming (modified after [77])

Microstreaming refers to the time-dependent oscillation of liquid molecules that are in close vicinity to the acoustically oscillating cavitation bubbles. Under compression and rarefaction cycles, oscillations in the cavitation bubbles cause rapid fluctuations in the magnitude and direction of the liquid movement. During the compression cycle, the cavitation bubbles shrink and the liquid molecules are pulled away from the membrane surface. On the other hand, during the rarefaction cycle, the cavitation bubbles expand and the liquid is pushed towards the membrane surface. The overall effect is to create significant shear or drag forces that possess the ability to remove foulants from the membrane surface. The effective range of microstreaming is small, typically in the range of 1-100 μm [77]. The concept of microstreaming is illustrated in Fig. 8.

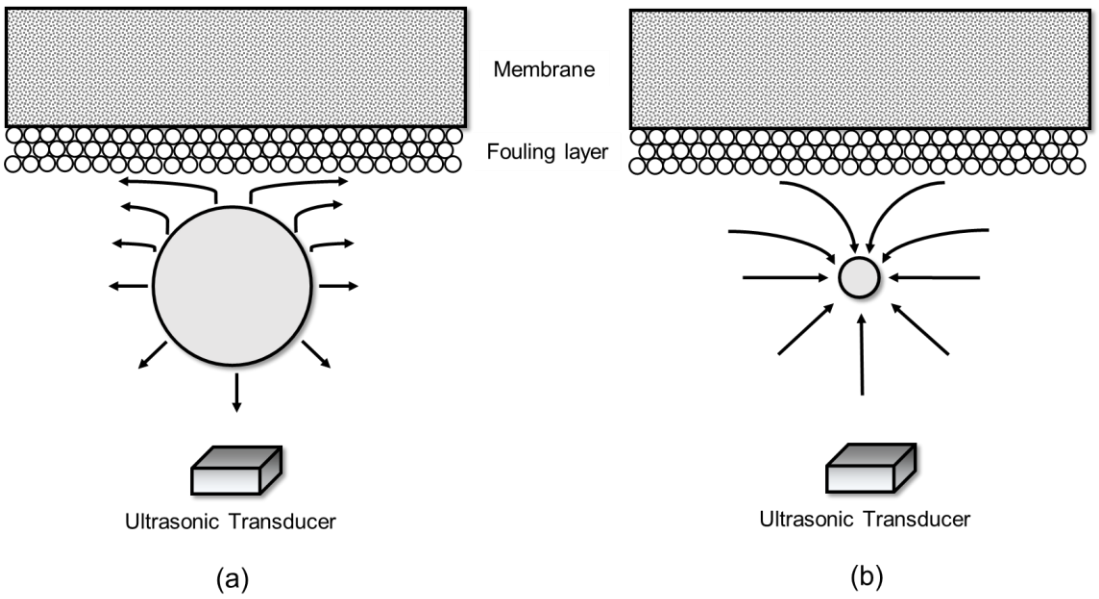

Fig. 8. Schematic representation of microstreaming (a) during bubble expansion (b) during bubble compression (modified after [77])

Microstreamers, shown in Fig. 9, are created as a result of standing waves that are formed by superimposition of the ultrasonic waves reflected from the solid membrane surface and the ultrasonic waves generated at the transducer. Due to Bjerkness forces, cavitation bubbles with size smaller than the resonance size are attracted by the antinodes of the standing waves. On the other hand, cavitation bubbles with size larger than the resonance size are accumulated at the nodes. While moving towards the antinodes, the cavitation bubbles follow a torturous path, form ribbon-like structures, and coalesce upon contact with one another [25,77]. The effective range of microstreamers is few millimeters while the velocity is approximately one order of magnitude higher than the average liquid velocity [77]. Microstreamers also play a role in detaching the foulants from the membrane surface when the antinodes on the membrane surface attract the cavitation bubbles [25,77].

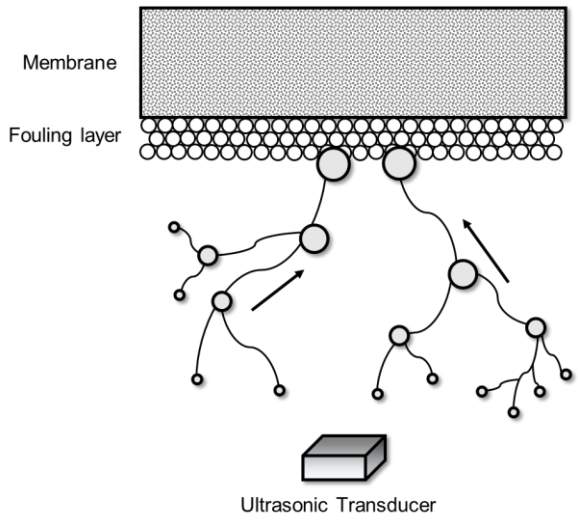

Fig. 9. Schematic representation of microstreamers (modified after [77])

In addition to microstreamers, the formation of microjets is also important in the release of particles from a fouled membrane. Microjets are formed as a consequence of asymmetric cavitation. When the cavitation bubbles are close to a solid membrane surface, the liquid movement in its vicinity decreases. This creates a differential pressure around the bubbles and a loss of the spherical bubble geometry [73]. Due to this differential pressure, the bubbles release strong water jets upon collapse. The velocity of the microjets is typically 100-200 ms^{-1} with an effective range on the order of the bubble diameter [77]. Given the high velocity, microjets possess an ability to remove foulants via pitting and erosion [25]. Fig. 10 depicts the formation of a microjet.

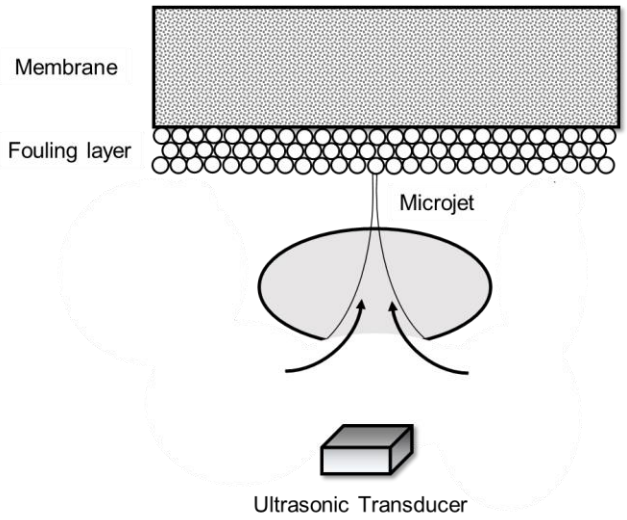

Fig. 10. Formation of a microjet after bubble collapse (modified after [77])

Finally, the generation of shock waves by ultrasound application is also important for removing particles from fouled membranes. Shock waves are continuously generated during the compression and rarefaction cycles. At the end of the compression cycle, the cavitation bubbles come to a sudden halt after reaching the minimum size. At this instant, the liquid molecules moving towards the bubbles are reflected which results in the generation of high pressure shock waves directed towards the membrane surface [73].

5. Application of ultrasound in membrane separation technologies

5.1. Flux enhancement and fouling control

The use of ultrasound for flux enhancement in UF and MF processes has been extensively investigated. However, studies related to ultrasound-assisted flux enhancement in NF, RO, MD, FO, and anaerobic MBR (AMBR) are so far limited. Table 2 summarizes the studies on ultrasound-assisted flux enhancement in different membrane-based separation processes.

Table 2

Summary of studies on ultrasound-assisted flux enhancement in membrane processes

Membrane process	Foulant solution	Membrane and apparatus details	Ultrasound details	Flux enhancement results	Reference
Ultrafiltration (UF)	Whey solution	Membrane: Flat sheet polysulfone (PS) and polyethersulfone (PES) Molecular weight cut-off (MWCO): 8-30 kDa Configuration: Cross-flow	Type: Ultrasonic bath and megasonic system Frequency: 50 kHz (continuous mode) and 1 MHz (pulsed mode)	For 8000 MWCO membrane, flux was enhanced by 60% using continuous sonication at TMP of 300 kPa and cross-flow velocity of 0.28 m/s	[30]
	Water from wastewater treatment plant of Salerno (Italy)	Membrane: Hollow fiber PS Pore size: 0.1 μm Configuration: Cross-flow	Type: Ultrasonic bath Frequency: 35 and 130 kHz	Fouling rate was reduced by 57.33% at a flux of 150 L/m^2 h and frequency of 35 kHz	[81]
	Bovine serum albumin (BSA)-lysozyme (Ly) binary protein mixture	Membrane: PS MWCO: 30 kDa Configuration: Cross-flow	Frequency: 25 kHz Power: 240 W	At pH 11, flux was enhanced by 135% and 120% with membrane in the upward and downward modes, respectively	[82]
	Dextran solution	Membrane: Flat PES MWCO: 30 kDa Configuration: Dead-end	Type: Ultrasonic bath Frequency: 28, 45, and 100 kHz	At the end of experiment, in comparison with the flux obtained without ultrasound application, the observed flux was 83% and 33% higher at ultrasound frequency of 28 kHz and 45 kHz, respectively. No flux enhancement was observed at 100 kHz frequency	[83]
	Synthetic clay solution	Membrane: Hollow fiber PS MWCO: 10 kDa Configuration: Cross-flow	Type: Immersed ultrasonic transducer Frequency: 40, 68, and 170 kHz Intensity: 3.1, 6.2, 9.2, and 12.3 kW/m^2	For TMP of 175 kPa, 33%, 20%, and 4% flux enhancement was obtained at 40, 68, and 170 kHz frequency, respectively	[84]

Surface water from Hoover Reservoir, Columbus, Ohio	Membrane: Flat sheet ceramic Anodisc™ – Al_2O_3 Pore size: 0.2 μm Configuration: Cross-flow	Type: Ultrasonic probe Frequency: 20 kHz	After 2 h, normalized flux increased from 0.21 in the absence of ultrasound to 0.70 with the aid of ultrasound	[85]
Whey solution	Membrane: Flat sheet PS MWCO: 30 kDa Configuration: Cross-flow	Type: Ultrasonic bath Frequency: 50 kHz Power: 2 W/L	Ratio of steady flux with ultrasound to steady flux without ultrasound was between 1.2 and 1.7 across the full range of experiments	[86]
Sulfate polystyrene latex particles	Membrane: Flat sheet polyvinylidene difluoride (PVDF) Pore size: 0.3 μm Configuration: Cross-flow	Type: Navy Type I lead zirconate titanate transducer Power: 0.8 W, 3.3 W, and 7.2 W	At pH 6.0 with 1 mM KCl and 10 mg/L sulfate latex particles, ratio of final flux (after 4 h) to initial clean water flux was 0.85 and 0.92 for applied powers of 0.8 W and 3.3 W, respectively. Membrane was damaged at 7.2 W	[87]
1 wt% dextran solution	Membrane: Flat sheet polyacrylonitrile (PAN) (8 wt% PAN and 15 wt% PAN) Pore size: 1 μm Configuration: Cross-flow	Type: Ultrasonic bath Frequency: 45 kHz Power: 248 W	Using 1 wt% solution of $2x10^6$ molecular weight dextran, 30 kPa pressure, and continuous sonification, no flux decline was observed during 80 min of operation	[88]
1 wt% dextran solution	Membrane: Flat sheet PAN Pore size: 1 μm Configuration: Cross-flow	Type: Ultrasonic bath Frequency: 28, 45, and 100 kHz Intensity: 2.7 W/cm^2	Using 1 wt% solution of $2x10^6$ molecular weight dextran, and 30 kPa pressure, no flux decline was observed during 80 min of operation at 28 and 45 kHz frequency. Flux improvement was negligible at 100 kHz frequency	[89]
Radix astragalus extract	Membrane: Flat sheet PES MWCO: 10 kDa Configuration: Dead-end	Type: Ultrasonic probe Frequency: 28, 45 and 100 kHz Power: 60, 90, and 120 W	At 20 kHz, using ultrasonic irradiation of 60, 90 and 120 W, observed fluxes were respectively 35%, 57% and 68% higher compared to the case without ultrasonic irradiation	[90]
Radix astragalus extract	Membrane: Hollow fiber PS module MWCO: 10 kDa	Type: Ultrasonic bath Frequency: 45 kHz Power: 30, 60, 90, and 120 W	At optimum conditions (continuous ultrasonic irradiation, power of 120 W, , TMP of 0.6 bar, and temperature of 20 ^oC), fouling rate was only 38.5–43% and process duration was 53–58 min	[91]
Skimmed milk powder	Membrane: Flat sheet PES Configuration: Cross-flow	Type: Ultrasonic bath Frequency: 37, 80 kHz and tandem Modes: Continuous, pulsed, sweeping, and degassing	Under best operating conditions (37 KHz and pulsed mode), flux enhancement was 187.4%	[92]
Water from wastewater treatment plant of Salerno (Italy)	Membrane: Single-fiber PS Pore size: 0.1 μm Configuration: Cross-flow	Type: Ultrasonic bath Frequency: 35 and 130 kHz Power: 5 W/L	35 kHz frequency was able to reduce the TMP increase by approximately 26%. However, 130 kHz frequency did not produce significant effects	[93]
Colloidal silica particles	Membrane: Flat ceramic Anodisc™ γ-Al_2O_3 Pore size: 0.2 μm Configuration: Cross-flow	Type: Ultrasonic probe Frequency: 20 kHz Intensity: 3.8 ± 0.1 W/cm^2	For 1.56 μm particles, the relative permeate flux improvement increased from 60% to 75% to 97% as the distance between the probe and the membrane	[94,95]

				surface decreased from 3.5 to 2.6 to 1.7 cm	
	Silica and NOM	Membrane: Flat ceramic Anodisc^{TM} γ-Al_2O_3 ceramic membrane Pore size: 0.2 μm Configuration: Cross-flow	Type: Ultrasonic probe Frequency: 20 kHz Power: 9.2 ± 0.4 W	With 8 mg/L NOM and 0.3 g/L silica particles at pH 9.2, normalized flux with ultrasonic irradiation was approximately four times higher at the end of the experiment	[96]
	Emulsification Wastewater	Membrane: Tubular ZrO_2 ceramic Pore size: 0.2 μm Configuration: Cross-flow, pilot-scale	Type: Ultrasonic probe Frequency: 21 kHz Power: 4, 8, 12, and 16 W	At optimum conditions (power of 8 W and 7 cm probe length), the steady flux with ultrasonic irradiation was three times higher than the steady flux without ultrasonic irradiation	[97]
	Paper industry wastewater (bark press filtrate and fabric press filtrate)	Membrane: Flat alumina-based ceramic Pore size: 0.12 μm Configuration: Dead-end	Type: Integrated ultrasonic transducer Frequency: 40 kHz Power: 200 and 400 W	At 200 W with bark press filtrate feed, the steady flux was approximately 2.5 times higher with ultrasonic irradiation applied from the feed side	[98]
Microfiltration (MF)	Paper industry wastewater (bark press filtrate and fabric press filtrate)	Membrane: Flat alumina-based ceramic Pore size: 0.75 μm Configuration: Dead-end	Type: Integrated ultrasonic transducer Frequency: 40 kHz Power: 200 and 400 W	At 400 W with bark press filtrate feed, the steady flux was approximately 6.1 times higher with ultrasonic irradiation applied from the permeate side. Application of ultrasound from the feed side resulted in the same steady flux as the one without ultrasound application	[98]
	Fresh cow milk	Membrane: Flat mixed cellulose ester Pore size: 0.2 μm Configuration: Dead-end	Type: Ultrasonic probes of different tip diameter Frequency: 20 kHz Power: 20, 40, and 50 W	Flux enhancement as high as 490% was observed. Compared to pulse irradiation, continuous ultrasound irradiation produced 33% higher flux enhancement	[99]
	1 wt% milk solution	Membrane: Hollow fiber polyethylene (PE) Pore size: 0.4 μm	Type: Ultrasonic bath Frequency: 28 kHz Power: 300 W	Flux enhanced up to 310% was obtained with membrane at 8 cm distance from the ultrasonic transducer and at 15 cm depth from water surface level	[100]
	Kraft paper mill effluent	Membrane: Flat sheet nylon Configuration: Cross-flow	Type: Ultrasonic horn Frequency: 28 kHz Power: 82.9 W/cm^2	After 30 min, flux with ultrasonic irradiation was 27.5% higher than the flux without ultrasonic irradiation. TMP and cross-flow velocity was 50 kPa and 0.125 m/s, respectively, in both cases	[101]
	Baker's yeast and BSA solution	Membrane: Tubular alumina-based ceramic Pore size: 0.04, 0.2, 0.8, 1.5, and 3 μm Configuration: Cross-flow	Type: Ultrasonic bath Frequency: 28 kHz	The steady flux was 4 to 6 times greater compared to the case without ultrasound. Cross-flow velocity, TMP, yeast concentration, and output power were 0.46 m/s, 40 kPa, 10 kg/m^3, and 240 W, respectively	[102]
Nanofiltration (NF)	Two-component dye and salt mixture	Membrane: Flat sheet hydrophilized polyamide (HPA) MWCO: 400 Configuration: Cross-flow	Type: Ultrasonic bath Frequency: 34 ± 3 kHz	With ultrasonic irradiation, the decline in permeate flux was not observed	[103]

Reverse osmosis (RO)	$CaSO_4$, Fe^{3+}, and carboxymethyl cellulose (CMC) solutions	Membrane: Flat sheet commercial polyamide-based Configuration: Cross-flow	Type: Ultrasonic bath Frequency: 20 kHz Intensity: 2.8 W/cm^2	On average, during the 3 h experiments, the permeate flux increased by about 50.8% for the 500 mg/L $CaSO_4$ solution, 69.7% for the 1000 mg/L $CaSO_4$ solution, 215% for the 20 mg/L Fe^{+3} solution, 264% for the 500 mg/L CMC solution, and 113% for the 1000 mg/L CMC solution	[104]
Forward osmosis (FO)	$CaSO_4$ and silica	Membrane: Flat sheet commercial cellulose acetate Configuration: Plate-and-frame module	Type: Ultrasonic probe Frequency: 72 kHz Power: 30 W	For $CaSO_4$ scaling, initial flux increased by 25% for ultrasound-assisted FO mode (UAFO) and by 166% for pressure and ultrasound-assisted FO mode (PUAFO). Permeate flux decline by colloidal fouling was only 21% for UAFO and 19% for PUAFO	[105]
	Sodium chloride solution	Membrane: Flat sheet commercial cellulose acetate Configuration: Cross-flow	Type: Ultrasonic bath	Flux increased up to 15% using ultrasound	[106]
	Tannin solution	Membrane: Flat sheet thin film composite polyamide on PS Configuration: Cross-flow	Type: Utrasonic transducer Frequency: 20 kHz Power: 50 and 100 W Mode: Pulsed and continuous	Flux was 1.2 times higher with continuous irradiation at 50 W, 2.2 times higher with continuous irradiation at 100 W, 2.1 times higher with pulsed irradiation (1 min on/1 min off) at 100 W, and 1.7 times higher with pulsed irradiation (1 min on/5 min off) at 100 W. ultrasound was applied from the feed side	[107]
	Sweet lime juice and rose extract anthocyanin	Membrane: Flat sheet commercial cellulose triacetate (CTA) Configuration: Cross-flow	Type: Ultrasonic bath Frequency: 30 kHz	Using ultrasound, initial flux was approximately 1.2 and 1.3 times higher for sweet lime juice and rose extract anthocyanin, respectively	[108]
Membrane distillation (MD)	$CaSO_4$, $CaCO_3$, and silica solutions	Membrane: Hollow fiber polytetrafluoroethylene (PTFE) hydrophobic Pore size: 0.26 µm Configuration: Direct contact	Type: Ultrasonic transducer Frequency: 20 kHz Power: 260 W	With $CaSO_4$ solution, ratio of flux to initial flux was maintained at 93% when the concentration factor reached 4.0 in the presence of ultrasonic irradiation. No flux decline was observed for $CaCO_3$ foulant (ultrasound, however, was not necessary). Ratio of flux to initial flux was maintained at 97% with silica foulant solution	[109]
	Sodium chloride solution	Membrane: Hollow fiber PTFE, polypropylene (PP), and PVDF Configuration: Direct contact	Type: Ultrasonic transducer Frequency: 20, 30, 40, and 68 kHz Power: 110 to 260 W	Ultrasonic irradiation produced permeate flux enhancement as high as 60%	[110]
	Tap water and sodium chloride solution	Membrane: Flat sheet PTFE Pore size: 1 µm Configuration: Air gap	Type: Ultrasonic horn Frequency: 20 and 38 kHz Power: Up to 90 W	Permeate flow rate with the ultrasonic irradiation increased up to 25% compared to the case without ultrasonic irradiation	[111]
	Silica solution	Membrane: Hollow fiber PTFE Pore size: 0.26 µm Configuration: Direct contact	Type: Ultrasonic transducer Frequency: 20 kHz Power: 110 to 260 W	Permeate flux was almost stable with ultrasonic irradiation and was enhanced by about 43%	[112]
Anaerobic membrane	Synthetic wastewater	Membrane: Follow fiber polyethylene (PE)	Type: Ultrasonic generator Frequency: 28 kHz	Membrane fouling	[113]

bioreactor (AMBR)		Pore size: 0.4 μm	Power: 60-150 W	was controlled such that membrane filtration resistance was constant $5x10^{11}$ m^{-1} for more than a week	
	Synthetic wastewater	Membrane: Follow fiber PE Pore size: 0.4 μm	Type: Ultrasonic generator Frequency: 28 kHz Intensity: 0.122 W/cm^2	The total filtration resistance was only 30% of that without ultrasonic irradiation after 28 days of operation	[114]
	Activated sludge	Membrane: Follow fiber PE Pore size: 0.4 μm	Type: Ultrasonic generator Frequency: 28 kHz Intensity: 0.18-0.5 W/cm^2	Cake layer resistance was 80.4% lower	[115]

Flux enhancement due to ultrasound application can be attributed to a number of effects. Cai *et al*. [83] showed that low-frequency ultrasound decreased the total fouling resistance (R_{tot}) and the reversible fouling resistance (R_{rev}) that is due to concentration polarization and cake layer, as depicted in Fig. 11. These results were obtained using dextran foulant solution and polyethersulfone (PES) membrane in a dead-end UF cell. The decrease in the resistance values was attributed to a decrease in concentration polarization effects due to acoustic streaming and cavitation effect induced by the ultrasound. Consequently, at the end of experiment, in comparison with the flux obtained without ultrasound application, the observed flux was 83% and 33% higher at ultrasound frequency of 28 kHz and 45 kHz, respectively. However, in this study, irreversible membrane fouling was negligible due the use of dextran as model foulant solution. Reduction in both reversible and irreversible fouling at suitable (low) ultrasound frequencies has been reported by Li *et al*. [84] during cross-flow UF of clay solution using hollow fiber polysulfone (PS) membrane. At TMP of 175 kPa, a flux enhancement of 33% was obtained using 48 kHz ultrasound frequency due to reduction in the fouling resistance. Similarly, ultrasound can reduce the filtration resistance in anaerobic MBR processes [113–115].

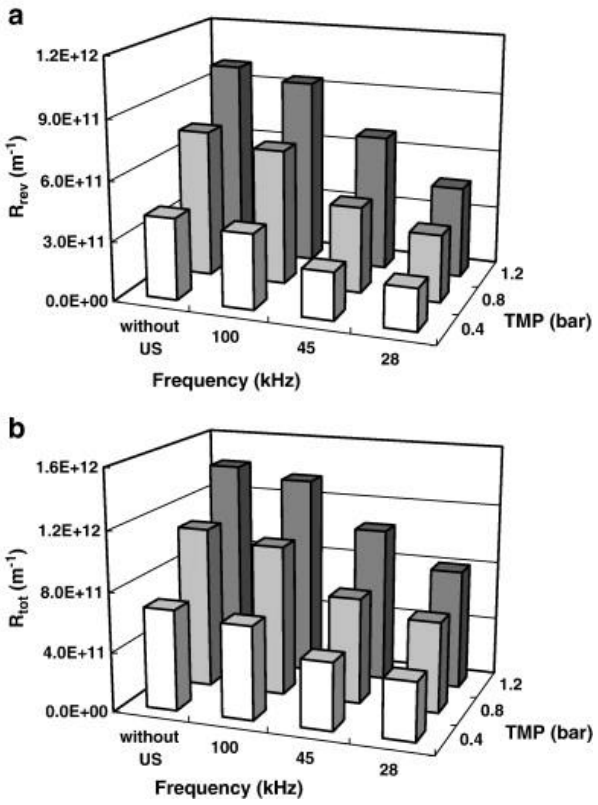

Fig. 11. Reduction in (a) reversible resistance and (b) total resistance at different values of ultrasonic frequency and TMP during dead-end UF of dextran foulant solution using PES membrane (adopted from [83])

Some studies have attributed flux enhancement to acoustic streaming and increased turbulence [92,94,96,103]. For example, using dextran foulant solution, Kobayashi and Fujii [89] showed that the flux enhancement in the studied UF process was due to acoustic streaming induced by low-frequency ultrasound that resulted in enhanced mass transfer of the permeate through the foulant layer. Similarly, Muthukumaran *et al*. [86] investigated the filtration of whey solution using a cross-flow UF apparatus and a PS membrane. The study reported that the flux enhancement was mainly due to acoustic streaming and mechanical vibrations rather than acoustic cavitation. At short times, flux decline was due to pore blockage. However, at longer times, flux decline was dominated by the cake layer growth. Ultrasound decreased the resistance of both the initial deposit layer and the growing cake as shown in Fig. 12 [86]. Overall, ratio of the steady flux with ultrasound to the steady flux without ultrasound was between 1.2 and 1.7 across the full range of experiments. However, Muthukumaran *et al*. [86] showed that ultrasound was unable to produce significant influence on pore blockage or internal fouling (Fig. 12). Cai *et al*. [91] also reported that ultrasound had no or little effect on adsorption and pore blocking of hollow fiber PS UF membrane.

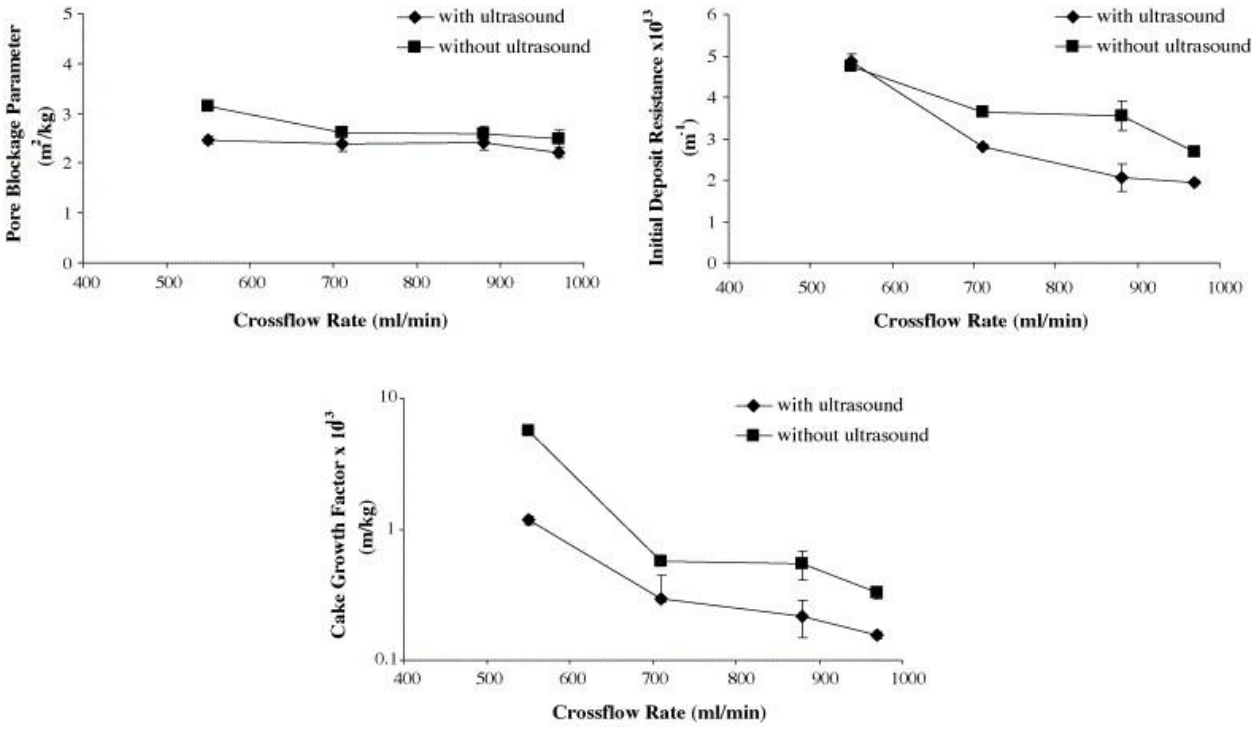

Fig. 12. Fouling parameters during cross-flow UF of 6 wt% whey solution using PS membrane. TMP and ultrasound intensity were 300 kPa and 2 W/L, respectively (adopted from [86])

In general, when the membrane is within the zone of acoustic cavitation, the flux is enhanced by combined effects of microstreaming, acoustic streaming, microjets, and the generation of microstreamers, microjets, and shock waves. However, outside the acoustic cavitation zone, acoustic streaming and increased turbulence are the main phenomena contributing to flux enhancement [95]. Lamminen *et al*. [87] enhanced the membrane flux by placing the UF system within the cavitation zone produced by the ultrasonic transducer. At pH 6.0 with 1 mM KCl and 10 mg/L sulfate latex particles as foulants, ratio of final flux (after 4 h) to initial clean water flux was 0.85 and 0.92 for applied powers of 0.8 W and 3.3 W, respectively. This suggests that the effects of fouling were almost completely mitigated. During inorganic fouling of commercial polyamide-based RO membrane with $CaSO_4$ solution, Feng *et al*. [104] concluded that microstreaming in the membrane pores and on the surface was the main cause of membrane cleaning and the consequent flux enhancement. On average, during the 3 h experiments, the permeate flux increased by about 50.8% for the 500 mg/L $CaSO_4$ solution, and 69.7% for the 1000 mg/L $CaSO_4$ solution by applying ultrasound with 20 kHz frequency.

Ultrasound irradiation may also enhance the flux partly by agglomerating small particles, thereby, reducing the probability of pore blockage. For instance, Borea *et al*. [81] used hollow fiber PS membrane to treat real wastewater in cross-flow UF process. Agglomeration of small suspended particles was observed due to generation of microstreamers and vibration. The agglomeration in the presence of ultrasound also resulted in higher turbidity removal compared to the turbidity removal in the absence of ultrasound. Similar agglomeration of particles in the UF process has been reported by Naddeo *et al*. [93].

In case of FO process, Choi *et al*. [105] successfully used ultrasound with 72 kHz frequency to decrease calcium sulfate scaling and silica colloidal fouling in a commercial cellulose acetate FO membrane. Ultrasound disassembled the calcium sulfate crystals and the silica colloids present in the feed solution. Ultrasound-assisted FO (UAFO) was found to outperform ultrasound-assisted FO (UAFO) in terms of flux enhancement. Compared to FO process without ultrasound, initial flux increased by 25% for UAFO and by 166% for UAFO in case of calcium sulfate scaling. In case of silica colloidal fouling, permeate flux decline was only 21% for UAFO and 19% for PUAFO compared to 50% flux decline in the case of FO without ultrasound. Heikkinen *et al*. [107] also reported ultrasound-assisted flux enhancement during FO filtration of tannin using a thin-film composite (TFC) membrane. In this study, flux enhancement was due to mitigation of concentration polarization in the porous support layer of the membrane. However, the reverse salt flux was also observed to be higher with ultrasound application.

Ultrasound can also mitigate calcium sulfate and silica colloid fouling in the MD process. In a study by Hou *et al*. [109] on direct contact MD, the ratio of flux to initial flux was maintained at 93% and 97% in case of calcium sulfate and silica fouling, respectively, due to the shock waves and microstreaming produced by the ultrasound. In addition, ultrasound can also enhance the flux by reducing the temperature polarization in the MD process [111,112].

There are several factors that influence the effectiveness of ultrasound-assisted flux enhancement. These factors are summarized below:

5.1.1. Ultrasound frequency

The effect of ultrasound frequency on flux enhancement has been thoroughly investigated. Lower ultrasound frequency is more effective in enhancing the flux since the cavitation bubbles are larger and the cavitational collapse is more violent leading to higher turbulence. Although higher ultrasound frequency increases the number of cavitation bubbles, the size of the bubbles is small

and the collapse is less violent. As a result, at higher frequencies, the flux enhancement and the fouling control rate are suppressed. For instance, at constant membrane flux, Borea *et al*. [81] observed that the membrane fouling rate decreased by 57.33% and 24.45% at 35 kHz and 130 kHz frequency, respectively, compared to the fouling rate in the UF process without ultrasound application. Fig. 13 depicts the effect of ultrasound frequency on the permeate flux over time during UF of dextran solution [83]. It is evident that low ultrasound frequency was more effective in enhancing the permeate flux. Similar effect of ultrasound frequency on flux enhancement has been observed in other studies [30,84,89,90,92,93,98,107,110].

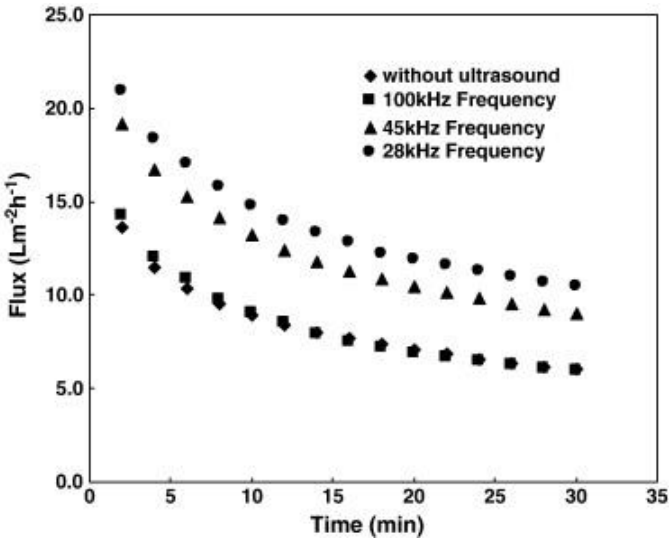

Fig. 13. Permeate flux in UF of dextran solution at TMP of 0.4 bar across PES membrane (adopted from [83])

5.1.2. Power intensity

Besides frequency, power or power intensity of the ultrasound also effects the flux enhancement. Generally, increasing the power intensity up to a certain maximum limit improves the flux enhancement. The power intensity cannot be increase indefinitely and a maximum power intensity value may exist beyond which the flux enhancement ceases or reduces or membrane damage occurs. For example, Matsumoto *et al*. [102] studied the effect of ultrasound power during MF of baker's yeast and BSA solution using alumina-based ceramic membranes of pore size 0.2 and 0.8 μm. As depicted in Fig. 14 [102], the steady-state permeate flux increased non-linearly with the applied power. At high power values, the effect on the steady-state flux was limited due to conversion of ultrasonic power to heat. Li *et al*. [97], on the other hand, studied the effect of ultrasound power on the UF of emulsification wastewater using ZrO_2 ceramic membrane. As

shown in Fig. 15 [97], the observed flux increased by increasing the ultrasound power from 4 W to 8 W. However, beyond 8 W, flux enhancement was reduced owing to increase in membrane fouling due to an increase in the emulsifying action and a decrease in the oil droplet size. The flux was, therefore, optimum at a power of 8 W, as shown in the inset of Fig. 15. Also, very high ultrasound power may lead to membrane damage. For example, Fig. 16 [84] shows the effect of ultrasound intensity during UF of clay solution using hollow fiber PS membrane. At the applied frequency of 40 kHz, a sudden dramatic increase in flux (at around 40 minutes) was observed when the power intensity was 12.3 kW/m^2. This sudden increase was attributed to membrane damage caused by the high power intensity.

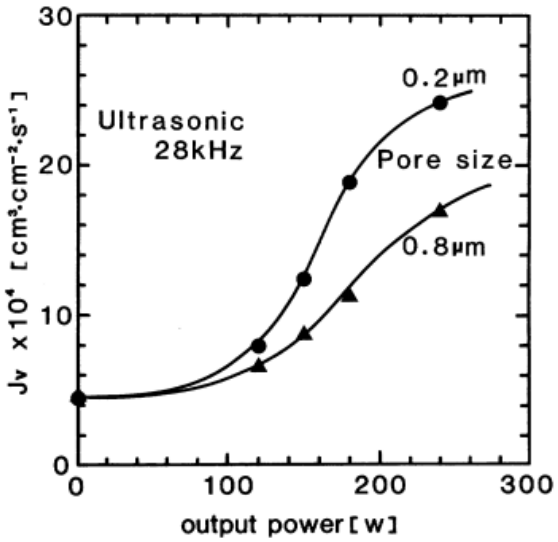

Fig. 14. Steady-state flux in MF of baker's yeast and BSA solution as a function of ultrasound power output. Results shown are for alumina-based ceramic membranes, TMP of 40 kPa, cross-flow velocity of 0.46 m/s, and yeast concentration of 10 kg/m^3 (adopted from [102])

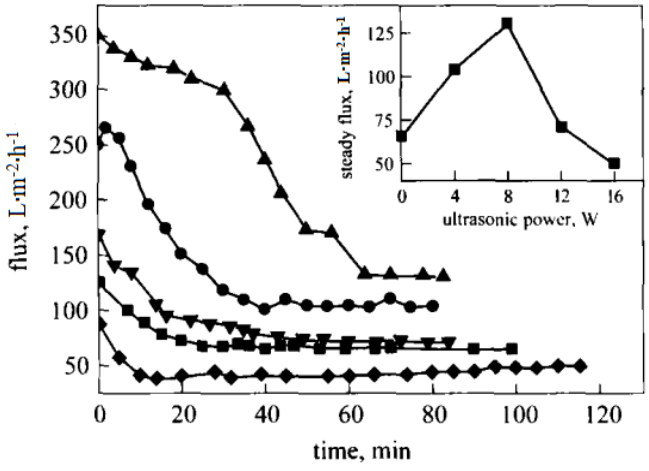

Fig. 15. Permeate flux in UF of emulsification wastewater as a function of ultrasound power (■ 0 W, ● 4 W, ▲ 8 W, ▼ 12 W, ♦ 16 W). Results shown are for ZrO_2 ceramic membrane (adopted from [97])

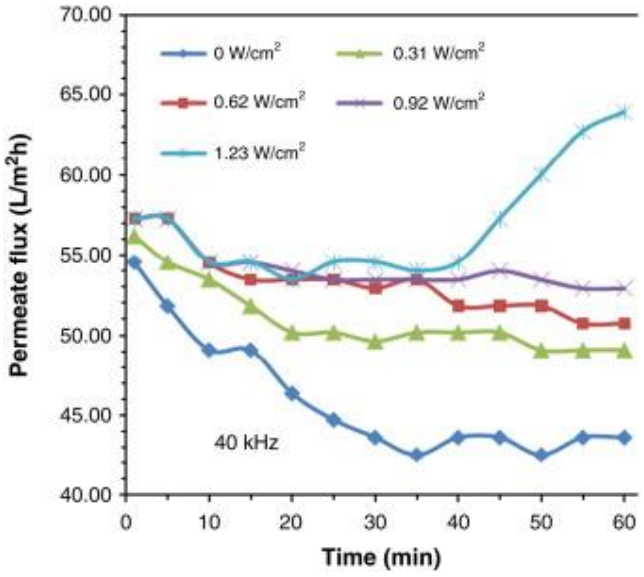

Fig. 16. Permeate flux in UF of clay solution as a function of ultrasound power intensity. Results shown are for hollow fiber PS membrane and 40 kHz frequency (adopted from [84])

5.1.3. Transmembrane pressure (TMP)

In pressure-driven membrane processes, TMP also plays an important role in ultrasound-assisted flux enhancement. From filtration point of view, higher filtration pressure naturally increases the permeate flux. However, this also results in higher drag force on the particles deposited on the membrane surface which exacerbates the fouling phenomenon. Also, higher filtration pressure compresses the cake layer, thereby, making its removal more difficult. At the same time, increasing the pressure increases the ultrasound intensity required to initiate cavitation and reduces the number of cavitation bubbles but results in more violent cavitational collapse. As a result, different relations between flux enhancement and TMP have been observed experimentally. Mirzaie and Mohammadi [99] observed that the ultrasound-assisted flux enhancement decreased from 228% to 27% when the pressure was increased from 0.5 to 1.4 bar. Muthukumaran *et al*. [86] reported that the ultrasound-assisted flux enhancement increased slightly with TMP. Kobayashi and Fujii [89] observed an increase in flux enhancement with increasing TMP while Matsumoto *et al*. [102] observed an optimum TMP at which the flux enhancement was maximum.

5.1.4. Feed solution properties

Flux enhancement by ultrasound is also affected by the feed solution properties. According to Muthukumaran *et al*. [86], ultrasound was effective in enhancing the flux even at high whey solution concentrations. Chen *et al*. [94] reported that ultrasound was more effective for flux enhancement with feeds that contain lower concentration and larger size of silica particles. At high particle concentrations, the presence of large number of particles increased the number of nuclei available for the generation of cavitation bubbles. This resulted in greater attenuation of ultrasound waves due to both scattering and absorption by the cavitation bubbles. The effect of ultrasound at high concentrations was, therefore, decreased. In addition, for small particles, the drag and lift forces created by the turbulence were found to be low. Therefore, ultrasound was more effective in enhancing flux when the feed contained larger particles. In another study, Chen *et al*. [96] studied the cross-flow UF of NOM and silica using Anodisc™ γ-Al_2O_3 ceramic membrane and 20 kHz ultrasound frequency. Higher flux enhancement was observed at higher pH in case of both NOM and NOM with silica particle filtration. This was attributed to changes in the surface charge of the membrane and the silica particles and changes in the shape of highly charged NOM macromolecules. In addition, in case of NOM filtration, higher flux enhancement was observed at low ionic strength of the feed. This is because, at low ionic strengths, the foulant-foulant and foulant-membrane interactions were more repulsive and allowed for easier fouling mitigation. Also, ultrasound-assisted flux enhancement was found to be less efficient when the feed contained Ca^{+2} ions. This was due to bridging among the deposited NOM macromolecules, silica particles, and the membrane that made the foulant layer more compact and the fouling mitigation more difficult. In another similar study, Chen *et al*. [85] observed that hydrophilic NOM was easier to remove by ultrasound than unfractionated NOM. In addition, ultrasound had little impact on flux improvement if the membrane was fouled with hydrophobic NOM.

5.1.5. Ultrasound mode

In the context of ultrasound-assisted flux enhancement, the use of intermittent mode of ultrasound irradiation has been investigated by several authors [90,92,95,99,102,103,107]. Typically, flux improvement decreases with long pulse intervals of ultrasound [95]. Although not as effective as continuous mode, intermittent mode may be the preferred choice since it reduces energy consumption. For example, Heikkinen *et al*. [107] reported 50% reduction in power consumption by using intermittent (1-min-on/1-min-off) ultrasound mode. At the same time, flux enhancement greater than 70% was still achievable.

5.2. Membrane cleaning

Besides its successful use in flux enhancement, ultrasound can be employed to clean fouled membranes. Several workers have investigated the application of ultrasound as a membrane cleaning technique. These studies are summarized in Table 3.

Ultrasound-assisted membrane cleaning can be performed in a number of ways. The membrane can be cleaned externally in the presence of ultrasound or cleaned within the filtration set-up using wash water or cleaning chemicals combined with ultrasound irradiation. Lamminen *et al*. [77] performed external batch cleaning by exposing Anodisc^{TM} γ-Al_2O_3 ceramic membranes to ultrasound inside a jacketed cleaning vessel containing water. The membranes were fouled with sulfate polystyrene latex particles. After performing the external cleaning, a full recovery of clean water flux was observed for all frequencies (except 1062 kHz) given that the ultrasonic treatment time and power intensity were above 30 s and 1.05 Wcm^{-2}, respectively. In another study, Lamminen *et al*. [87] used an external ultrasonic cleaning vessel, containing 1mM KCl solution, to clean Anodisc^{TM} γ-Al_2O_3 ceramic and polyvinylidene difluoride (PVDF) membranes. The membranes were almost fully cleaned and the water flux after cleaning was very close to the initial clean water flux of the new membranes.

Kobayashi *et al*. [116] cleaned PS UF and cellulose MF membranes within the filtration cell by combining water washing with ultrasound. The PS and cellulose membranes were first fouled by peptone solution and milk solution, respectively. At 28 kHz frequency, complete and partial cleaning was achieved for the PS and the cellulose membrane, respectively. Similar procedure has been used to clean membranes in other studies [83,117,118]. Li *et al*. compared three different methods to clean nylon MF membrane fouled by Kraft paper mill effluent. The methods included forward flushing, ultrasonic cleaning, and ultrasonic cleaning combined with forward flushing. The resulted indicated that the cleaning efficiency was the highest (97.8%) when ultrasound was used in combination with forward flushing.

Table 3

Summary of studies on ultrasound-assisted membrane cleaning

Membrane process	Foulant solution	Membrane and apparatus details	Ultrasound details	Cleaning efficiency results	Reference
Ultrafiltration (UF)	Sulfate polystyrene latex particles	Membrane: Flat Anodisc^{TM} γ-Al_2O_3 ceramic Pore size: 0.2 μm Configuration: Dead-end	Type: Ultrasonic transducer Frequency: 70, 205, 354, 620, and 1062 kHz	A full recovery in clean water flux was observed for all frequencies (except 1062 kHz) when ultrasonic treatment times exceeded 30 s and power intensities were greater than 1.05 Wcm^{-2}. Cleaning was better when the fouled surface faced the transducer	[77]

Dextran solution	Membrane: Flat PES MWCO: 30 kDa Configuration: Dead-end	Type: Ultrasonic bath Frequency: 28, 45, and 100 kHz	Membrane was effectively cleaned. Flux recovery was highest at the lowest frequency of 28 kHz	[83]
Sulfate polystyrene latex particles	Membrane: Flat PVDF and ceramic Anodisc™ γ-alumina Pore size: 0.3 μm for PVDF and 0.2 μm for ceramic Configuration: Dead-flow	Type: Navy Type I lead zirconate titanate transducer	For ceramic membrane, the cleaned flux ratio (ultrasonically cleaned flux/initial pure water flux) was 0.93 at 37.0 W and 0.97 at 60.1 W. For PVDF membrane, the cleaned flux ratio was almost 1.0 at 12.2 W. Membrane damage occurred above 12.2 W	[87]
Peptone solution	Membranes: Flat sheet PS MWCO: 10 kDa Configuration: Cross-flow	Type: Ultrasonic bath Frequency: 28, 45 and 100 kHz Intensity: 23 W/cm^2	28 kHz frequency achieved complete water cleaning of the fouled membrane	[116]
Diary whey	Membrane: Flat sheet PS MWCO: 30 kDa Configuration: Cross-flow	Type: Ultrasonic bath Frequency: 50 kHz	Ultrasound increased the flux recovery up to 112% depending on the experimental conditions	[117]
Peptone solution	Membranes: Flat sheet PS and PAN (8 and 15 wt% PAN) MWCO: 10 kDa for PS Configuration: Cross-flow	Type; Ultrasonic bath Frequency: 45 kHz Intensity: 2.73 W/cm^2	Permeate was fully recovered by sonication, water cleaning, and water cleaning under sonication but longer time was required for PS membrane	[118]
1 wt% skim milk solution	Membrane: Spiral wound PES MWCO: 10 kDa Configuration: Cross-flow	Type: Ultrasonic bath Frequency: 28, 45, and 100 kHz	No remarkable enhancement of flux was observed after ultrasound irradiation. However, the cleaning efficiency of ultrasound and ethylenediamintetraacetic acid (EDTA) increased when applied altogether. The best results were obtained when mixed waveform of ultrasound and 3 mM EDTA were used together	[119]
Lactic acid fermentation broth	Membrane: Flat PVDF MWCO: 100 kDa Configuration: Dead-end	Frequency: 100 kHz	The normalized permeate flux (ratio of flux after cleaning to initial flux) reached to 97.5% when 1% of the mixture of sodium hydroxide and sodium hypochlorite was used with the assistance of 100 kHz ultrasound	[120]
Copper (Cu)–polyethylenimine (PEI) solution and water-oil (w/o) emulsions	Membrane: Flat Amicon YM10 MWCO: 10 kDa Configuration: Dead-end	Type: Ultrasonic horn Frequency: 20 kHz	In case of Cu-PEI solution, flux recovery was 30%, 50%, and 70% (relative to pure water flux) using an ultrasonic power of 30, 57, and 93 W, respectively, at ultrasonic horn tip height of 20 mm. At power of 145 W and tip height of 65mm, about 30% of the flux was recovered for a w/o solution with 15% emulsification and w/o volume fraction of 1.0	[121]
Calcium chloride ($CaCl_2$) solution	Membrane: Polluted PVDF Configuration: Hollow fiber module	Type: Flat plate transducer	With a synergistic effect of ultrasound and 2 g/L citric acid aqueous solution, 81% of flux was recovered about	[122]
Diary whey	Membrane: Flat sheet PS MWCO: 30 kDa Configuration: Cross-flow	Type: Ultrasonic bath Frequency: 50 kHz	Effect of ultrasound on NaOH chemical cleaning was studied. Ultrasound	[123]

				increased the cleaning efficiency under all experimental conditions, typically by 5-10%	
	BSA solution	Membrane: Flat sheet PES MWCO: 5 and 30 kDa Configuration: Cross-flow	Type: Ultrasonic bath Frequency: 20, 25, 30, and 38 kHz	Ultrasound-assisted chemical cleaning was performed using NaOH. An enhancement of 9-12% in the flux recovery was observed	[124]
	Yeast solution	Membrane: Flat sheet cellulose acetate MWCO: 15-30 kDa Configuration: Cross-flow	Type: Focused ultrasonic beams Frequency: 671 kHz	Filtration rate was partially restored	[125]
	Reactive Black 5 (RB5) dye solution	Membrane: INSIDE CéRAM® multichannel tubular ceramic MWCO: 150 kDa Configuration: Cross-flow	Type: Ultrasonic bath Frequency: 37 and 80 kHz and mixed wave	The maximum predicted cleaning efficiency was 32.19% under optimum conditions	[126]
Microfiltration (MF)	Kraft paper mill effluent	Membrane: Flat sheet nylon Configuration: Cross-flow	Type: Horn transducer Frequency: 20 kHz Intensity: 82.9 W/cm^2	Cleaning efficiency was 97.8% with ultrasound combined with forward flushing	[101]
	1% milk solution	Membranes: Flat sheet cellulose Pore size: 0.2 µm Configuration: Cross-flow	Type: Ultrasonic bath Frequency: 28, 45 and 100 kHz Intensity: 23 W/cm^2	At 28 kHz ultrasound irradiation with water washing, flux was almost 4 times higher compared to the flux obtained with water washing alone	[116]
	Peptone solution	Membranes: Flat sheet PVDF Pore size: 0.2 µm Configuration: Cross-flow	Type; Ultrasonic bath Frequency: 45 kHz Intensity: 2.73 W/cm^2	Permeate flux was fully recovered in three steps: sonication, water cleaning, and water cleaning under sonication	[118]
	Synthetic raw water	Membranes: Flat PTFE Pore size: 0.5 µm Configuration: Dead-end	Type: Ultrasonic probe Frequency: 20 kHz Power: 50 W	Maximum flux recovery was 83.24%	[127]
	NOM	Membrane: Flat PTFE Pore size: 0.6 µm Configuration: Dead-end	Type: Ultrasonic probe Power: 5 and 15 W	Using probe distance of 2 cm and coagulant dose of 15 mg/L, 45% flux recovery was obtained with continuous ultrasound irradiation for 25 min at 15 W	[128]
	1 wt% milk solution	Membrane: Flat sheet PVDF Pore size: 0.2 µm Configuration: Cross-flow	Type: Ultrasonic bath Frequency: 28, 45, and 100 kHz	Combined cleaning with 3 mMole EDTA and 28 kHz ultrasound irradiation achieved the highest cleaning efficiency	[129]
Nanofiltration (NF)	Arsenic-rich brackish water	Membrane: Flat aromatic polyamide (NF3A) Configuration: Cross-flow	Type: Ultrasonic bath Frequency: 40 kHz Intensity: 1 W/cm^2	Recovery of water flux reached 99.99% using citric acid cleaning (pH of 3.0) with ultrasound	[130]

Some studies have investigated ultrasound-assisted chemical cleaning of membranes. For example, Maskooki *et al*. [119] carried out cleaning experiments using a combination of ultrasound and EDTA chelating agent. Skimmed milk solution was used as foulant solution for spiral wound PES UF membrane. A synergistic effect was observed when ultrasound and EDTA were used simultaneously. The best results were obtained when mixed waveform of ultrasound

and 3 mM EDTA were used together. Also, the study reported that only 5 min forward flushing under ultrasound and sequestering agent EDTA was sufficient and additional cleaning was unnecessary. Similar results were found in another study by Maskooki *et al*. [129] where synergistic effect was observed when ultrasound was used with EDTA for cleaning of PVDF MF membrane fouled with 1% milk solution.

Wei *et al*. [122] cleaned polluted PVDF hollow fiber membranes using 2 g/L citric acid. In the presence of ultrasound, the permeate flux recovery increased to 81% compared to 66.3% recovery with 2 g/L citric acid alone. Also, Wang *et al*. [130] applied ultrasound-assisted citric acid cleaning to aromatic polyamide NF membrane. Ultrasound combined with water flushing could only recover the membrane water flux by around 75%. However, recovery of water flux reached 99.99% using citric acid cleaning (pH of 3.0) combined with ultrasound. Similar synergetic effects have been observed with other chemical cleaning agents. Wang *et al*. [120] a comparative study for cleaning of PVDF UF membrane using deionized water, NaOH, NaClO, and a mixture of NaOH and NaClO in the absence and presence of ultrasound. The highest normalized permeate flux (97.5%) was achieved when 1% mixture of NaOH and NaClO was used with 100 kHz ultrasound frequency. Luján-Facundo *et al*. [124] and Alventosa-deLara *et al*. [126] also reported an increase in NaOH cleaning efficiency in the presence of ultrasound.

There are several factors that influence the effectiveness of ultrasound-assisted membrane cleaning. Many authors have studied the effect of ultrasound frequency on the membrane cleaning efficiency. Similar to the case of ultrasound-assisted flux enhancement, lower ultrasound frequency has been reported to be more effective in membrane cleaning. Fig. 17 shows the effect of ultrasound frequency on water washing of PS UF membrane fouled by peptone solution [116]. Clearly, compared to 45 and 100 kHz frequencies, the clean water flux was almost fully recovered using ultrasound with 28 kHz frequency. Similarly, lower frequency was found to be more effective in water cleaning of PES UF membrane fouled with dextran solution [83].

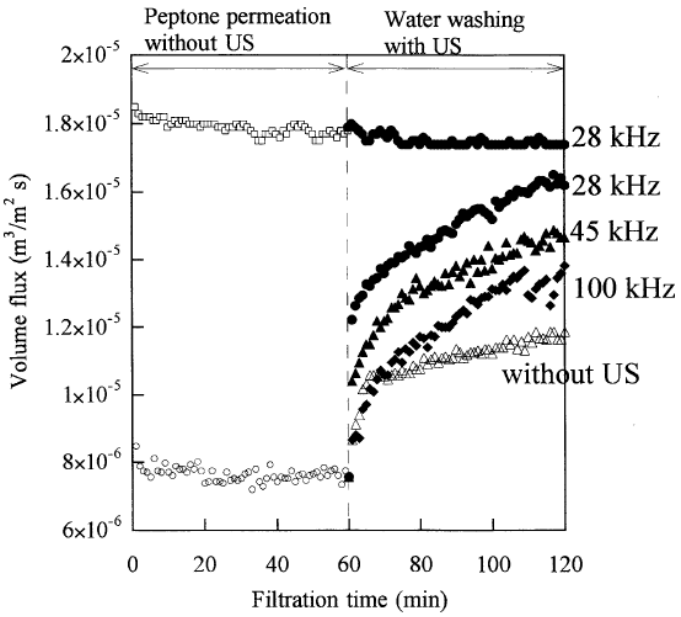

Fig. 17. Permeate flux vs. filtration time for fouling and water washing cleaning periods of PS UF membrane at different ultrasound frequencies (intensity: 23 W/cm^2). Fouling experiment was performed using 0.5 wt% peptone solution. (○ permeate flux with peptone solution, □ clean water flux, US refers to ultrasound) (adopted from [116])

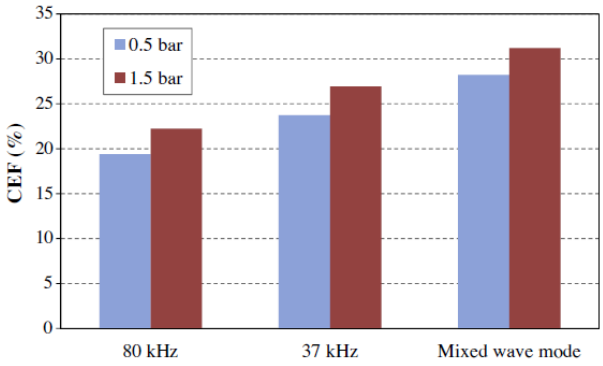

Fig. 18. Cleaning efficiency (CEF) using 37 kHz, 80 kHz, and mixed wave mode ultrasound. Results are for INSIDE CéRAM® multichannel tubular ceramic membrane fouled with Reactive Black 5 (RB5) dye solution. Operating conditions during cleaning: cross-flow velocity of 3 m/s, temperature of 40 ^{o}C, and power level at 70% (adopted from [126])

Some authors considered the effect of mixed wave ultrasound (combination of low and high frequency) on the membrane cleaning efficiency. For example, Alventosa-deLara *et al*. [126] reported that higher cleaning efficiency was observed when mixed wave mode ultrasound was applied during water rinsing of INSIDE CéRAM® multichannel tubular ceramic membrane fouled

by Reactive Black 5 (RB5) dye solution (shown in Fig. 18). Similar results have been observed in other studies [119,129]. In the mixed wave mode, large number of small bubbles are created during the high frequency stage. These bubbles are then collapsed violently during the low frequency stage. As a result, the cleaning efficiency increases due to combined action of violent collapse and large number of bubbles [126].

Few studies have focused on the effect of ultrasound power on membrane cleaning [87,117,123,126]. Typically, the cleaning efficiency improves with increasing the ultrasound power. However, very high power levels can lead to membrane damage. Besides ultrasound power, temperature of the cleaning solution also effects the cleaning efficiency. Li *et al*. [101] observed higher cleaning efficiency at low temperatures during ultrasound-assisted water cleaning of nylon MF membrane fouled by Kraft paper mill effluent (Fig. 19). However, Chai *et al*. [118] observed the opposite trend and the cleaning efficiency increased at higher temperatures (Fig. 20). Using aromatic polyamide NF membrane fouled by arsenic-rich brackish water, Wang *et al*. [130] reported an optimum temperature at which the ultrasound-assisted citric acid cleaning efficiency was maximum (Fig. 21). These conflicting results were observed since both foulant properties and cavitation effects depend on temperature. Cavitational collapse is more violent at low temperatures. However, the solution viscosity decreases at low temperatures which does not allow for easy formation of the cavitation bubbles. At the same time, foulant properties such as solubility and diffusivity are temperature dependent. Therefore, the overall effect of temperature on the cleaning efficiency is dictated by the relative importance of all these factors.

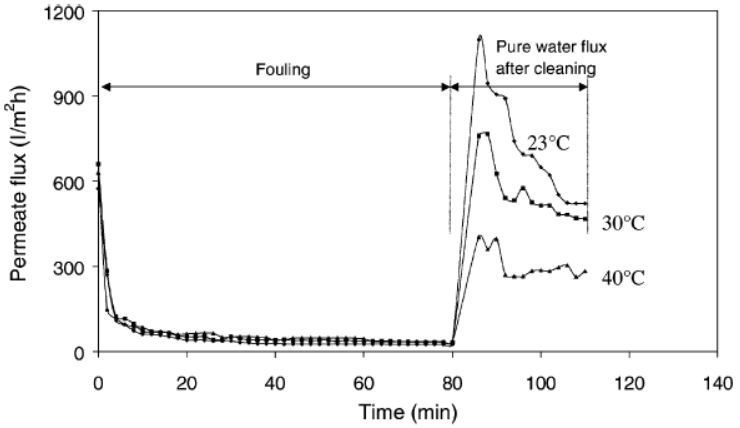

Fig. 19. Effect of cleaning water temperature on flux recovery of nylon MF membrane fouled with Kraft paper mill effluent. Results shown are for ultrasound frequency of 20 kHz, intensity of 82.9 W/cm^2, cross-flow velocity of 0.125 m/s, and TMP of 50 kPa (adapted from [101])

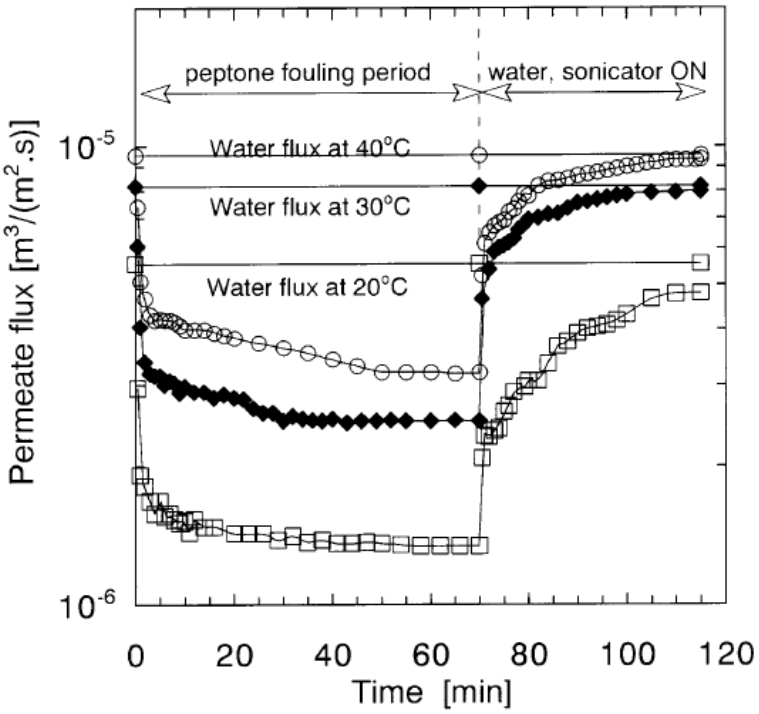

Fig. 20. Effect of cleaning water temperature on flux recovery of PS UF membrane fouled peptone solution. Results shown are for ultrasound frequency of 45 kHz and intensity of 2.73 W/cm^2 (adapted from [118])

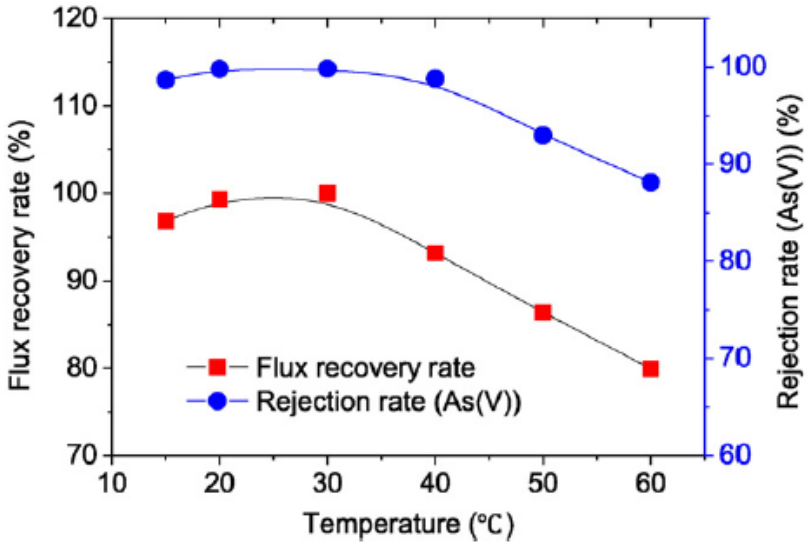

Fig. 21. Effect of temperature on flux recovery during ultrasound-assisted citric acid cleaning of aromatic polyamide NF membrane fouled with arsenic-rich brackish water. Results shown are for ultrasound frequency of 40 kHz and intensity of 1 W/cm^2 (adapted from [130])

Ultrasound-assisted cleaning efficiency also depends on TMP during the cleaning process. Some studies showed lower cleaning efficiency at higher TMP values [123,130] while the opposite trend was observed in another study [126]. These conflicting results can be explained by the effect of pressure on the acoustic cavitation and the foulant cake layer compression as explained in Section 5.1.3.

5.3. Ultrasound in desalination pretreatment processes

Numerous modifications to desalination membranes have been proposed in order to enhance their performance and thus reduce membrane fouling. Several studies have investigated the use of turbulence in the filtration units and its effect on improving back-transport and thus increasing the shear rate near the membrane surface, which would eventually lead to preventing particle deposition and reducing fouling [131]. The use of ultrasound technology has been proved to be an effective pretreatment technique for suppressing algal growth and biofilm which reduces the formation of biofouling on the RO/UF membranes [131-133]. Yet, studies related to the application of ultrasound as a sole pretreatment for membrane desalination techniques are limited and not fully understood. Generally, ultrasound is used for deactivating and deagglomerating bacterial clusters through physical, mechanical and chemical effects as a result of acoustic cavitation, where the cavitation bubbles produces energy to mechanically disrupt the bacteria in the feed solution. Few studies have shown that the application of ultrasound technology can be a powerful water disinfection solution, however, achieving a complete bacterial kill rates and destruction of pollutants using ultrasound alone would require a high ultrasonic intensities which makes it a relatively expensive alternative especially for large-scale microbiological decontamination [134]. Some microorganisms have shown significant resistant to conventional disinfection techniques used such as biocide, chlorination, UV light and thermal treatment, thus, ultrasound technology is used in combination with some of these conventional techniques and leads to significant reduction in the amount of bacteria in water samples [135].

In a study conducted by Joyce *et al*. [134], the effect of power ultrasound on Bacillus subtilis activity was investigated. Bacillus subtilis produces colonies that agglomerates in spherical clusters which provides protection against biocide treatment. Different ultrasound frequencies and powers (20 - 38 kHz) and (512 - 850 kHz) were investigated on the kill rates of Bacillus species. Results showed that the application of ultrasound has two impacts on the activity of Bacillus subtilis suspensions: bacterial de-clumping and bacterial killing. The use of low frequency ultrasound or high power ultrasound leads to an increase in the bacterial kill rates, whereas the

use of high frequency ultrasound or low intensity ultrasound leads to de-clumping of bacterial cells with a low kill rates.

Ultrasound can be used in combination with chlorination for reducing the number of bacterial cells present in water. It can also reduce the amount of chlorine used for water disinfection. According to Phull *et al*. [135] high power ultrasound is a suitable water treatment and disinfection process due to its ability to destruct bacterial cells, reduce the chlorine content in water efficiently (90 to 20 mg/L within 15 min of sonication), reduce the amount of chlorine required for water disinfection, reduce the sewage effluents particle sizes from 40 to 1 g, and enhance the effect of conventional chlorination.

Bacteria and algae growth can be controlled through a treatment process combining shear, micro-bubbles, and high-frequency low-power ultrasound. According to Broekman *et al*. [136] sessile and planktonic biological growth can be effectively controlled due to the high stress environment formed by ultrasonic waves which in stabilize and reduce the biofilms formed. This treatment process reduces the need for chemical biocides for water disinfection and leads to achieving a chemical-free microbial control for water systems using low-power, high-frequency ultrasound waves.

In case of UF, Koh *et al.* [131] successfully used ultrasound with a 20 KHz frequency in combination with heat treatment as a pretreatment for whey solutions: WPC80 solution and fresh whey solution in order to improve downstream ultrafiltration performance. Results showed that sonication alone had a small but significant effect on membrane fouling, however, the use of heat pretreatment in combination with ultrasound reduced the membrane pore blockage and foulant cake growth significantly especially at higher solid concentrations.

Another study investigated the membrane filtration hybrid process combined with ultrasonication for dairy wastewater treatment. Kerte´sz *et al*. [137] and his colleagues have tested 20 and 50 kDa molecular weight cut-off polyethersulfone ultrafiltration membranes with both continuous and half intermittent ultrasonic irradiation for the reduction of dairy wastewater treatment organic load. Results in Fig. 22 indicated that the highest average flux was attained under continuous ultrasonication and was pronounced clearly for the 50 kDa membrane. Four different filtration laws (Equations 13 - 16) were plotted against the measured data, Fig. 22 indicates that the best correlation among the four linearized filtration laws were attained by plotting the cake filtration.

Complete pore blocking: $J = J_0 e^{-K_b t}$ (13)

Gradual pore blocking: $J = J_0\left(1 + \frac{1}{2}K_s(AJ_0)^{0.5}\,t\right)^{-2}$ (14)

Intermediate filtration: $J = J_0(1 + K_i A J_0 t)^{-1}$ (15)

Cake filtration: $J = J_0(1 + 2K_c(AJ_0)^2\,t)^{-0.5}$ (16)

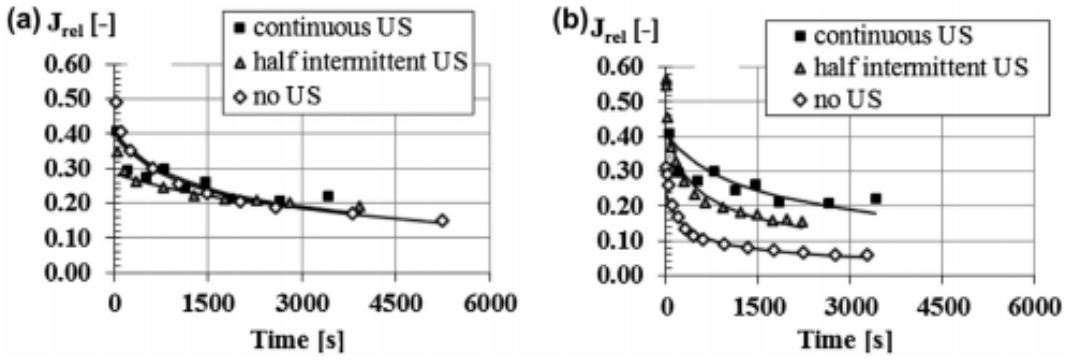

Fig. 22. Ultrafiltration membranes relative fluxes: (a) 20 kDa membrane and (b) 50 kDa membrane (adapted from [137])

Moreover, ultrasound technology can be used as a feedwater pretreatment of an RO system. In a study conducted by Al-juboori *et al.* [132] a 55 kHz (horn type) ultrasound batch configuration reactor was utilized where different levels of ultrasonic intensity, pressure, temperature and treatment time in sonication, thermosonication and manosonication treatments were used for E.coli deactivation. The ultrasound treatment efficiency was evaluated based on the measured permeate flux as well as the biofilm formed on the RO membrane. Results showed that the best E. coli disruption is attained through thermosonication treatment where 103 CFU/mL of the E. coli were eliminated.

6. Challenges in industrial application of ultrasound

Despite the effectiveness of ultrasound in enhancing flux and membrane cleaning, practical application of ultrasound in membrane-based separation processes is faced by some key challenges. One of these major challenges is related to membrane damage. Upon exposure to ultrasound, the membrane may be susceptible to damage owing to extreme cavitational collapse depending on the frequency and power intensity of the ultrasound and the irradiation time period. Some studies have reported membrane damage and loss of membrane integrity upon exposure to ultrasound [84,95,122,138,139]. The power intensity of ultrasound must be controlled to

minimize both membrane damage and energy consumption. Masselin *et al*. [138] conducted a detailed study on the effect of 47 kHz ultrasound on polymeric membranes. Three types of polymeric membranes were used: PES (MWCO: 3, 10, 30, and 100 kDa), PVDF (MWCO: 40 kDa), and polyacrylonitrile (PAN) (MWCO: 40 and 50 kDa). After a total ultrasonic treatment duration of 2 h, only PES membranes were found to be affected over the entire surface while PAN (50 kDa) and PVDF (40 kDa) were affected only on the edges. All membrane, except PAN (40 kDa), exhibited large variations in water permeability with membrane degradation mostly occurring within the first 5 min of ultrasound exposure. Fig. 23 shows the microscopic images of the PES (100 kDa) membrane after 2 h of ultrasound treatment.

Wang *et al*. [139] studied the effect of 40 kHz ultrasound on polymeric MF membranes. The membranes included PES, nylon 6 (N_6), mixed ester of cellulose nitrate and cellulose acetate (CN-CA), and PVDF. At power intensity of 2.13 W/cm^2, all membranes except PVDF exhibited some degree of damage resulting in increased water flux after 60 min of exposure to ultrasound. PVDF membrane only exhibited damage at an intensity of 3.7 W/cm^2 after 90 min exposure. Chen *et al*. [95] also reported damage to ceramic Anodisc^{TM} γ-Al_2O_3 membrane after 5 min of sonication at 20 kHz. The damage was observed in the form of pitting on the membrane surface caused by shock waves and microjets. Wei *et al*. [122] reported that PVDF hollow fiber UF membrane was damaged within 6 min after exposure to ultrasound with 8.68 kW/m^2 power intensity. The number of studies on ultrasound-induced membrane damage are limited. Different membrane materials have different resistance to damage during ultrasonic treatment. As a result, further experimental work is required to evaluate the effect of ultrasound on the integrity of membranes composed of different materials.

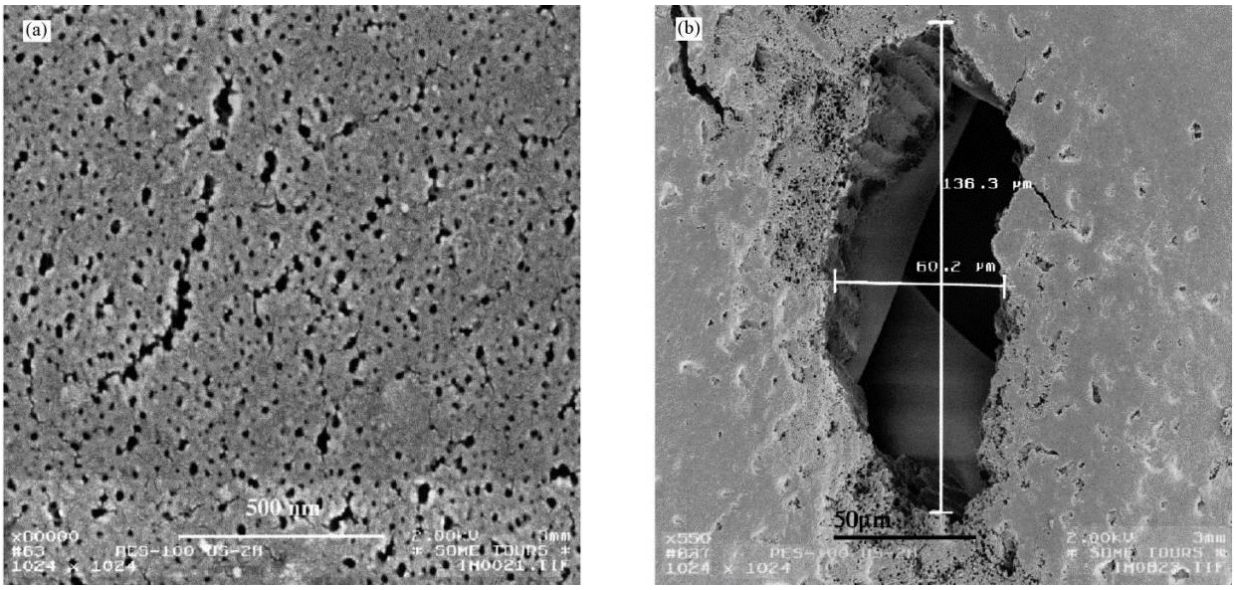

Fig. 23. Microscopic images of PES (100 kDa) membrane after 2 h treatment with 47 kHz ultrasound (a) membrane surface at magnification of 80,000 (b) highly damaged area under magnification of 550 (adapted from [138])

Industrialization of ultrasound-assisted membrane processes is another key challenge. Almost all studies on the use of ultrasound for flux enhancement and membrane cleaning have been conducted using laboratory-scale cross-flow units. Despite the large number of such studies, successful commercial application of ultrasound technology requires detailed studies on large-scale membrane processes which are essentially non-existent. This necessitates research investigations into the effectiveness of ultrasound in flux enhancement and cleaning of full scale membrane modules.

Although there is no scientific or research disagreement that ultrasound is promising in enhancing flux and membrane cleaning, the economic effectiveness and feasibility is a challenge that still needs to be addressed. Depending on the operating conditions, the ultrasound power requirements may be high enough to limit its applicability on an industrial scale. However, so far, there are no studies on the economics of the ultrasound-assisted membrane-based or membrane cleaning processes. The economic feasibility of ultrasound-assisted flux enhancement and membrane cleaning, therefore, requires immediate attention.

The source of ultrasound presents another key challenge in successful application of ultrasound in large-scale membrane processes. Most studies have relied on the use of ultrasonic baths, probes, or horns. All of these ultrasound sources are likely to be ineffective in large-scale

applications. Therefore, investigations on ultrasound transducer technologies are highly important.

Further experimental work is required to study the effectiveness of ultrasound in flux enhancement and cleaning of different types of membrane modules. Most studies have focused only on flat sheet membranes while only few studies have used hollow fiber or spiral wound membranes where ultrasound application is more tedious owing to the membrane configuration. There is also a research gap in studying the effect of ultrasound on flux enhancement and cleaning of membranes other than MF and UF membranes. Lack of such important studies poses a serious challenge to the adoption of ultrasound-assisted membrane processes on industrial scale.

7. Concluding remarks

This review paper summarizes the major research efforts related to ultrasound-assisted flux enhancement and membrane cleaning. Based on the experimental results reviewed in this study, ultrasound appears to be an effective means of flux enhancement and membrane cleaning since it possesses a unique ability to generate special chemical and physical effects that can remove foulants from the membrane surface. However, ultrasound application cannot produce significant influence on pore blockage and is only limited to external fouling. Despite its effectiveness in flux enhancement and membrane cleaning, ultrasound-assisted membrane technology is still in its infancy owing to some serious limitations. These limitations include large-scale application, lack of suitable transducers, and lack of data on economic feasibility. Further research investigations are required to study the effect of ultrasound on membrane damage, evaluate the effectiveness of ultrasound application for membranes other than flat-sheet type, and analyze the economics of ultrasound-assisted membrane processes.

References

[1] G. Amy, N. Ghaffour, Z. Li, L. Francis, R.V. Linares, T. Missimer, all authored are required, Membrane-based seawater desalination: Present and future prospects, Desalination. 401 (2017) 16–21. doi:10.1016/j.desal.2016.10.002.

[2] W.L. Ang, a. W. Mohammad, a. Benamor, N. Hilal, Hybrid coagulation-NF membrane processes for brackish water treatment: Effect of pH and salt/calcium concentration, Desalination. 390 (2016) 25–32. doi:10.1016/j.desal.2016.03.018.

[3] H. Dong, L. Zhao, L. Zhang, H. Chen, C. Gao, W.S. Winston Ho, High-flux reverse osmosis membranes incorporated with NaY zeolite nanoparticles for brackish water desalination, J. Memb. Sci. 476 (2015) 373–383. doi:10.1016/j.memsci.2014.11.054.

[4] P.S. Goh, T. Matsuura, a. F. Ismail, N. Hilal, Recent trends in membranes and membrane processes for desalination, Desalination. 391 (2016) 43–60. doi:10.1016/j.desal.2015.12.016.

[5] K.P. Lee, T.C. Arnot, D. Mattia, A review of reverse osmosis membrane materials for desalination-Development to date and future potential, J. Memb. Sci. 370 (2011) 1–22. doi:10.1016/j.memsci.2010.12.036.

[6] J. Zuo, S. Bonyadi, T.S. Chung, Exploring the potential of commercial polyethylene membranes for desalination by membrane distillation, J. Memb. Sci. 497 (2016) 239–247. doi:10.1016/j.memsci.2015.09.038.

[7] A.C. Bortoluzzi, J. a. Faitão, M. Di Luccio, R.M. Dallago, J. Steffens, G.L. Zabot, all authored are required, Dairy wastewater treatment using integrated membrane systems, J. Environ. Chem. Eng. 5 (2017) 4819–4827. doi:10.1016/j.jece.2017.09.018.

[8] F. Jia, Y. Yin, J. Wang, Removal of cobalt ions from simulated radioactive wastewater by vacuum membrane distillation, Prog. Nucl. Energy. 103 (2018) 20–27. doi:10.1016/j.pnucene.2017.11.008.

[9] F. Li, H. Jiahui, Q. Xia, M. Lou, B. Yang, Q. Tian, all authored are required, Direct contact membrane distillation for the treatment of industrial dyeing wastewater and characteristic pollutants, Sep. Purif. Technol. 195 (2017) 83–91. doi:10.1016/j.seppur.2017.11.058.

[10] N. Singh, I. Petrinic, C. Hélix-Nielsen, S. Basu, M. Balakrishnan, Concentrating molasses distillery wastewater using biomimetic forward osmosis (FO) membranes, Water Res. 130 (2018) 271–280. doi:10.1016/j.watres.2017.12.006.

[11] S. You, J. Lu, C.Y. Tang, X. Wang, Rejection of heavy metals in acidic wastewater by a novel thin-film inorganic forward osmosis membrane, Chem. Eng. J. 320 (2017) 532–538. doi:10.1016/j.cej.2017.03.064.

[12] S. Zhao, J. Minier-Matar, S. Chou, R. Wang, A.G. Fane, S. Adham, Gas field produced/process water treatment using forward osmosis hollow fiber membrane:

Membrane fouling and chemical cleaning, Desalination. 402 (2017) 143–151. doi:10.1016/j.desal.2016.10.006.

[13] C. Bhattacharjee, V.K. Saxena, S. Dutta, Watermelon juice concentration using ultrafiltration: Analysis of sugar and ascorbic acid, Food Sci. Technol. Int. 23 (2017) 637–645. doi:10.1177/1082013217714672.

[14] C. Bhattacharjee, V.K. Saxena, S. Dutta, Fruit juice processing using membrane technology: A review, Innov. Food Sci. Emerg. Technol. 43 (2017) 136–153. doi:10.1016/j.ifset.2017.08.002.

[15] G. Brans, C.G.P.H. Schroën, R.G.M. Van Der Sman, R.M. Boom, Membrane fractionation of milk: State of the art and challenges, J. Memb. Sci. 243 (2004) 263–272. doi:10.1016/j.memsci.2004.06.029.

[16] S. Gunko, S. Verbych, M. Bryk, N. Hilal, Concentration of apple juice using direct contact membrane distillation, Desalination. 190 (2006) 117–124. doi:10.1016/j.desal.2005.09.001.

[17] C. a. Quist-Jensen, F. Macedonio, C. Conidi, a. Cassano, S. Aljlil, O. a. Alharbi, all authored are required, Direct contact membrane distillation for the concentration of clarified orange juice, J. Food Eng. 187 (2016) 37–43. doi:10.1016/j.jfoodeng.2016.04.021.

[18] H. V. Adikane, R.K. Singh, S.N. Nene, Recovery of penicillin G from fermentation broth by microfiltration, J. Memb. Sci. 162 (1999) 119–123. doi:10.1016/S0376-7388(99)00129-5.

[19] M.P. Belleville, P. Lozano, J.L. Iborra, G.M. Rios, Preparation of hybrid membranes for enzymatic reaction, Sep. Purif. Technol. 25 (2001) 229–233. doi:10.1016/S1383-5866(01)00106-X.

[20] U.B. Finger, J. Thömmes, D. Kinzelt, M.R. Kula, Application of thiophilic membranes for the purification of monoclonal antibodies from cell culture media, J. Chromatogr. B Biomed. Sci. Appl. 664 (1995) 69–78. doi:10.1016/0378-4347(94)00362-9.

[21] I. Pinnau, L.G. Toy, Solid polymer electrolyte composite membranes for olefin/paraffin separation, J. Memb. Sci. 184 (2001) 39–48. doi:10.1016/S0376-7388(00)00603-7.

[22] M. Takht Ravanchi, T. Kaghazchi, A. Kargari, Application of membrane separation processes in petrochemical industry: a review, Desalination. 235 (2009) 199–244. doi:10.1016/j.desal.2007.10.042.

[23] W. Guo, H.H. Ngo, J. Li, A mini-review on membrane fouling, Bioresour. Technol. 122 (2012) 27–34. doi:10.1016/j.biortech.2012.04.089.

[24] A. Sonune, R. Ghate, Developments in wastewater treatment methods, Desalination. 167 (2004) 55–63. doi:10.1016/j.desal.2004.06.113.

[25] S. Muthukumaran, S.E. Kentish, G.W. Stevens, M. Ashokkumar, Application of ultrasound in membrane separation processes: A review, Rev. Chem. Eng. 22 (2006) 155–194. doi:10.1515/REVCE.2006.22.3.155.

[26] D.M. Kanani, X. Sun, R. Ghosh, Reversible and irreversible membrane fouling during in-line microfiltration of concentrated protein solutions, J. Memb. Sci. 315 (2008) 1–10. doi:10.1016/j.memsci.2008.01.053.

[27] a. L. Ahmad, N.F. Che Lah, S. Ismail, B.S. Ooi, Membrane antifouling methods and alternatives: Ultrasound approach, Sep. Purif. Rev. 41 (2012) 318–346. doi:10.1080/15422119.2011.617804.

[28] R. Field, Fundamentals of Fouling, in: K.-V. Peinemann, S. Pereira (Eds.), Membr. Technol. Membr. Water Treat., Wiley-VCH Verlag GmbH & Co. KGaA, Weinheim, Germany, 2010: pp. 1–23. doi:10.1002/9783527631407.ch1.

[29] S. Sablani, M. Goosen, R. Al-Belushi, M. Wilf, Concentration polarization in ultrafiltration and reverse osmosis: A critical review, Desalination. 141 (2001) 269–289. doi:10.1016/S0011-9164(01)85005-0.

[30] S. Muthukumaran, S.E. Kentish, G.W. Stevens, M. Ashokkumar, R. Mawson, The application of ultrasound to dairy ultrafiltration: The influence of operating conditions, J. Food Eng. 81 (2007) 364–373. doi:10.1016/j.jfoodeng.2006.11.008.

[31] M.C. Porter, Handbook of Industrial Membrane Technology, Noyes Publications, 1990.

[32] B. Malczewska, M.M. Benjamin, Efficacy of hybrid adsorption/membrane pretreatment for low pressure membrane, Water Res. 99 (2016) 263–271. doi:10.1016/j.watres.2016.04.065.

[33] Z. Yin, C. Yang, C. Long, A. Li, Effect of integrated pretreatment technologies on RO membrane fouling for treating textile secondary effluent: Laboratory and pilot-scale experiments, Chem. Eng. J. 332 (2018) 109–117. doi:10.1016/j.cej.2017.09.059.

[34] P.S. Goh, W.J. Lau, M.H.D. Othman, a. F. Ismail, Membrane fouling in desalination and its mitigation strategies, Desalination. 425 (2018) 130–155. doi:10.1016/j.desal.2017.10.018.

[35] K.Y. Jee, D.H. Shin, Y.T. Lee, Surface modification of polyamide RO membrane for improved fouling resistance, Desalination. 394 (2016) 131–137. doi:10.1016/j.desal.2016.05.013.

[36] J. Ayyavoo, T.P.N. Nguyen, B.M. Jun, I.C. Kim, Y.N. Kwon, Protection of polymeric membranes with antifouling surfacing via surface modifications, Colloids Surfaces A Physicochem. Eng. Asp. 506 (2016) 190–201. doi:10.1016/j.colsurfa.2016.06.026.

[37] B.D. McCloskey, H.B. Park, H. Ju, B.W. Rowe, D.J. Miller, B.D. Freeman, A bioinspired fouling-resistant surface modification for water purification membranes, J. Memb. Sci. 413-414 (2012) 82–90. doi:10.1016/j.memsci.2012.04.021.

[38] J.R. Du, S. Peldszus, P.M. Huck, X. Feng, Modification of membrane surfaces via microswelling for fouling control in drinking water treatment, J. Memb. Sci. 475 (2015) 488–495. doi:10.1016/j.memsci.2014.10.040.

[39] I.D. Huner, H.A. Gulec, Fouling behavior of poly (ether) sulfone ultrafiltration membrane during concentration of whey proteins : Effect of hydrophilic modification using atmospheric pressure argon jet plasma, Colloids Surfaces B Biointerfaces. 160 (2017) 510–519. doi:10.1016/j.colsurfb.2017.10.003.

[40] Z.F. Cui, S. Chang, a. G. Fane, The use of gas bubbling to enhance membrane processes, J. Memb. Sci. 221 (2003) 1–35. doi:10.1016/S0376-7388(03)00246-1.

[41] W. Zhang, J. Luo, L. Ding, M.Y. Jaffrin, A review on flux decline control strategies in pressure-driven membrane processes, Ind. Eng. Chem. Res. 54 (2015) 2843–2861. doi:10.1021/ie504848m.

[42] N. Porcelli, S. Judd, Chemical cleaning of potable water membranes: A review, Sep. Purif. Technol. 71 (2010) 137–143. doi:10.1016/j.seppur.2009.12.007.

[43] X. Shi, G. Tal, N.P. Hankins, V. Gitis, Fouling and cleaning of ultrafiltration membranes: A review, J. Water Process Eng. 1 (2014) 121–138. doi:10.1016/j.jwpe.2014.04.003.

[44] A. Sagiv, R. Semiat, Backwash of RO spiral wound membranes, Desalination. 179 (2005) 1–9. doi:10.1016/j.desal.2004.11.050.

[45] H.M. Kyllönen, P. Pirkonen, M. Nyström, Membrane filtration enhanced by ultrasound: A review, Desalination. 181 (2005) 319–335. doi:10.1016/j.desal.2005.06.003.

[46] X.M. Wang, T.D. Waite, Impact of gel layer formation on colloid retention in membrane filtration processes, J. Memb. Sci. 325 (2008) 486–494. doi:10.1016/j.memsci.2008.08.016.

[47] L. Song, Flux decline in crossflow microfiltration and ultrafiltration: Mechanisms and modeling of membrane fouling, J. Memb. Sci. 139 (1998) 183–200. doi:10.1016/S0376-7388(97)00263-9.

[48] W. Yuan, A.L. Zydney, Humic acid fouling during microfiltration, J. Memb. Sci. 157 (1999) 1–12. doi:10.1016/S0376-7388(98)00329-9.

[49] L. Fan, J.L. Harris, F.A. Roddick, N.A. Booker, Influence of the characteristics of natural organic matter on the fouling of microfiltration membranes, Water Res. 35 (2001) 4455–4463. doi:10.1016/S0043-1354(01)00183-X.

[50] L.D. Tijing, Y.C. Woo, J.S. Choi, S. Lee, S.H. Kim, H.K. Shon, Fouling and its control in membrane distillation-A review, J. Memb. Sci. 475 (2015) 215–244. doi:10.1016/j.memsci.2014.09.042.

[51] V. Discart, M.R. Bilad, S. Van Nevel, N. Boon, J. Cromphout, I.F.J. Vankelecom, Role of transparent exopolymer particles on membrane fouling in a full-scale ultrafiltration plant:

Feed parameter analysis and membrane autopsy, Bioresour. Technol. 173 (2014) 67–74. doi:10.1016/j.biortech.2014.08.098.

[52] Y. Yu, S. Lee, S. Hong, Effect of solution chemistry on organic fouling of reverse osmosis membranes in seawater desalination, J. Memb. Sci. 351 (2010) 205–213. doi:10.1016/j.memsci.2010.01.051.

[53] A.S. Tawfik, K.G. Vinod, Nanomaterial and Polymer Membranes: Synthesis, Characterization, and Applications, 1st ed., Elsevier, 2016.

[54] S. Shirazi, C.J. Lin, D. Chen, Inorganic fouling of pressure-driven membrane processes - A critical review, Desalination. 250 (2010) 236–248. doi:10.1016/j.desal.2009.02.056.

[55] S. Lee, C.H. Lee, Effect of operating conditions on CaSO4 scale formation mechanism in nanofiltration for water softening, Water Res. 34 (2000) 3854–3866. doi:10.1016/S0043-1354(00)00142-1.

[56] W. Rudolfs, J.L. Balmat, Colloids in Sewage: I. Separation of Sewage Colloids with the Aid of the Electron, Source Sew. Ind. Wastes. 24 (1952) 247–256. doi:10.1016/S0262-1762(99)80122-9.

[57] S.G. Yiantsios, D. Sioutopoulos, A.J. Karabelas, Colloidal fouling of RO membranes: An overview of key issues and efforts to develop improved prediction techniques, Desalination. 183 (2005) 257–272. doi:10.1016/j.desal.2005.02.052.

[58] C.Y. Tang, T.H. Chong, A.G. Fane, Colloidal interactions and fouling of NF and RO membranes: A review, Adv. Colloid Interface Sci. 164 (2011) 126–143. doi:10.1016/j.cis.2010.10.007.

[59] I. Huisman, C. Trägårdh, Particle transport in crossflow microfiltration I. Effects of hydrodynamics and diffusion, Chem. Eng. Sci. 54 (1999) 271–280. doi:10.1016/S0009-2509(98)00222-X.

[60] K.J. Howe, M.M. Clark, Fouling of microfiltration and ultrafiltration membranes by natural waters, Environ. Sci. Technol. 36 (2002) 3571–3576. doi:10.1021/es025587r.

[61] X. Zhu, M. Elimelech, Fouling of Reverse Osmosis Membranes by Aluminum Oxide Colloids, J. Environ. Eng. 121 (1995) 884–892. doi:10.1061/(ASCE)0733-9372(1995)121:12(884).

[62] M. Elimelech, X. Zhu, A.E. Childress, S. Hong, Role of membrane surface morphology in colloidal fouling of cellulose acetate and composite aromatic polyamide reverse osmosis membranes, J. Memb. Sci. 127 (1997) 101–109. doi:10.1016/S0376-7388(96)00351-1.

[63] E.M. Vrijenhoek, S. Hong, M. Elimelech, Influence of membrane surface properties on initial rate of colloidal fouling of reverse osmosis and nanofiltration membranes, J. Memb. Sci. 188 (2001) 115–128. doi:10.1016/S0376-7388(01)00376-3.

[64] R. Komlenic, Rethinking the causes of membrane biofouling, Filtr. Sep. 47 (2010) 26–28. doi:10.1016/S0015-1882(10)70211-1.

[65] V. Kochkodan, N. Hilal, A comprehensive review on surface modified polymer membranes for biofouling mitigation, Desalination. 356 (2015) 187–207. doi:10.1016/j.desal.2014.09.015.

[66] T. Nguyen, F.A. Roddick, L. Fan, Biofouling of water treatment membranes: A review of the underlying causes, monitoring techniques and control measures, Membranes (Basel). 2 (2012) 804–840. doi:10.3390/membranes2040804.

[67] K. Yasui, Acoustic Cavitation and Bubble Dynamics, 1st ed., Springer International Publishing, Cham, 2018. doi:10.1007/978-3-319-68237-2.

[68] J. Luo, Z. Fang, R.L. Smith, Jr., X. Qi, Fundamentals of Acoustic Cavitation in Sonochemistry, in: Z. Fang, R.L. Smith, Jr., X. Qi (Eds.), Prod. Biofuels Chem. with Ultrasound, 1st ed., Springer Science, Dordrecht, 2015: pp. 3–33.

[69] T.Y. Wu, N. Guo, C.Y. Teh, J.X.W. Hay, Theory and Fundamentals of Ultrasound, in: Adv. Ultrasound Technol. Environ. Remediat., Springer, Dordrecht, 2013: pp. 5–12. doi:10.1007/978-94-007-5533-8.

[70] J.P. Lorimer, T.J. Mason, Sonochemistry. Part 1—The physical aspects, Chem. Soc. Rev. 16 (1987) 239–274. doi:10.1039/CS9871600239.

[71] Y.L. Pang, A.Z. Abdullah, S. Bhatia, Review on sonochemical methods in the presence of catalysts and chemical additives for treatment of organic pollutants in wastewater, Desalination. 277 (2011) 1–14. doi:10.1016/j.desal.2011.04.049.

[72] T. Leong, M. Ashokkumar, K. Sandra, The fundamentals of power ultrasound - A review, Acoust. Aust. 39 (2011) 54–63. doi:ISSN 0814-6039.

[73] V.S. Moholkar, H.A. Choudhury, S. Singh, S. Khanna, A. Ranjan, S. Chakma, all authored are required, Physical and Chemical Mechanisms of Ultrasound in Biofuel Synthesis, in: Z. Fang, R.L. Smith, Jr., X. Qi (Eds.), Prod. Biofuels Chem. with Ultrasound, 1st ed., Springer, Dordrecht, 2014: pp. 35–86. doi:10.1007/978-94-017-9624-8.

[74] Y.T. Shah, A.B. Pandit, V.S. Moholkar, Cavitation Reaction Engineering, Kluwer Academic/Plenum Press, New York, 1999.

[75] S.K. Bhangu, M. Ashokkumar, Theory of Sonochemistry, Top. Curr. Chem. 374 (2016) 56. doi:10.1007/s41061-016-0054-y.

[76] T.G. Leighton, The Acoustic Bubble, Academic Press, San Diego, 1994.

[77] M.O. Lamminen, H.W. Walker, L.K. Weavers, Mechanisms and factors influencing the ultrasonic cleaning of particle-fouled ceramic membranes, J. Memb. Sci. 237 (2004) 213–223. doi:10.1016/j.memsci.2004.02.031.

[78] L.H. Thompson, L.K. Doraiswamy, Sonochemistry: Science and Engineering, Ind. Eng. Chem. Res. 38 (1999) 1215–1249.

[79] M.S. Pham, T.-D. Shrestha, R. Amatya, Ultrasound Technology in Green Chemistry, Springer, Dordrecht, 2011. doi:10.1007/978-94-007-2409-9.

[80] Yusuf G. Adewuyi, Sonochemistry: Environmental Science and Engineering Applications, Ind. Eng. Chem. Res. (2001) 4681–4715. doi:10.1021/ie010096l.

[81] L. Borea, V. Naddeo, M.S. Shalaby, T. Zarra, V. Belgiorno, H. Abdalla,. all authored are required, Wastewater treatment by membrane ultrafiltration enhanced with ultrasound: Effect of membrane flux and ultrasonic frequency, Ultrasonics. 83 (2018) 42–47. doi:10.1016/j.ultras.2017.06.013.

[82] M.Y. Teng, S.H. Lin, R.S. Juang, Effect of ultrasound on the separation of binary protein mixtures by cross-flow ultrafiltration, Desalination. 200 (2006) 280–282. doi:10.1016/j.desal.2006.03.338.

[83] M. Cai, S. Zhao, H. Liang, Mechanisms for the enhancement of ultrafiltration and membrane cleaning by different ultrasonic frequencies, Desalination. 263 (2010) 133–138. doi:10.1016/j.desal.2010.06.049.

[84] X. Li, J. Yu, a. G.A. Nnanna, Fouling mitigation for hollow-fiber UF membrane by sonication, Desalination. 281 (2011) 23–29. doi:10.1016/j.desal.2011.07.036.

[85] Y. Gao, D. Chen, L.K. Weavers, H.W. Walker, Ultrasonic control of UF membrane fouling by natural waters: Effects of calcium, pH, and fractionated natural organic matter, J. Memb. Sci. 401-402 (2012) 232–240. doi:10.1016/j.memsci.2012.02.009.

[86] S. Muthukumaran, S.E. Kentish, M. Ashokkumar, G.W. Stevens, Mechanisms for the ultrasonic enhancement of dairy whey ultrafiltration, J. Memb. Sci. 258 (2005) 106–114. doi:10.1016/j.memsci.2005.03.001.

[87] M.O. Lamminen, H.W. Walker, L.K. Weavers, Cleaning of particle-fouled membranes during cross-flow filtration using an embedded ultrasonic transducer system, J. Memb. Sci. 283 (2006) 225–232. doi:10.1016/j.memsci.2006.06.034.

[88] X. Chai, T. Kobayashi, N. Fujii, Ultrasound effect on cross-flow filtration of polyacrylonitrile ultrafiltration membranes, J. Memb. Sci. 148 (1998) 129–135. doi:10.1016/S0376-7388(98)00145-8.

[89] T. Kobayashi, X. Chai, N. Fujii, Ultrasound enhanced cross-flow membrane filtration, Sep. Purif. Technol. 17 (1999) 31–40. doi:10.1016/S1383-5866(99)00023-4.

[90] M. Cai, S. Wang, Y. Zheng, H. Liang, Effects of ultrasound on ultrafiltration of Radix astragalus extract and cleaning of fouled membrane, Sep. Purif. Technol. 68 (2009) 351–356. doi:10.1016/j.seppur.2009.06.013.

[91] M. Cai, S. Wang, H.H. Liang, Optimization of ultrasound-assisted ultrafiltration of Radix astragalus extracts with hollow fiber membrane using response surface methodology, Sep. Purif. Technol. 100 (2012) 74–81. doi:10.1016/j.seppur.2012.09.002.

[92] M. Hashemi Shahraki, A. Maskooki, A. Faezian, Effect of various sonication modes on permeation flux in cross flow ultrafiltration membrane, J. Environ. Chem. Eng. 2 (2014) 2289–2294. doi:10.1016/j.jece.2014.10.005.

[93] V. Naddeo, L. Borea, V. Belgiorno, Sonochemical control of fouling formation in membrane ultrafiltration of wastewater: Effect of ultrasonic frequency, J. Water Process Eng. 8 (2015) e92–e97. doi:10.1016/j.jwpe.2014.12.005.

[94] D. Chen, L.K. Weavers, H.W. Walker, Ultrasonic control of ceramic membrane fouling: Effect of particle characteristics, Water Res. 40 (2006) 840–850. doi:10.1016/j.watres.2005.12.031.

[95] D. Chen, L.K. Weavers, H.W. Walker, Ultrasonic control of ceramic membrane fouling by particles: Effect of ultrasonic factors, Ultrason. Sonochem. 13 (2006) 379–387. doi:10.1016/j.ultsonch.2005.07.004.

[96] D. Chen, L.K. Weavers, H.W. Walker, J.J. Lenhart, Ultrasonic control of ceramic membrane fouling caused by natural organic matter and silica particles, J. Memb. Sci. 276 (2006) 135–144. doi:10.1016/j.chroma.2005.10.025.

[97] L. Shu, W. Xing, N. Xu, Effect of Ultrasound on the Treatment of Emulsification Wastewater by Ceramic Membranes, Chinese J. Chem. Eng. 15 (2007) 855–860. doi:10.1016/S1004-9541(08)60014-2.

[98] H. Kyllönen, P. Pirkonen, M. Nyström, J. Nuortila-Jokinen, A. Grönroos, Experimental aspects of ultrasonically enhanced cross-flow membrane filtration of industrial wastewater, Ultrason. Sonochem. 13 (2006) 295–302. doi:10.1016/j.ultsonch.2005.04.006.

[99] A. Mirzaie, T. Mohammadi, Effect of ultrasonic waves on flux enhancement in microfiltration of milk, J. Food Eng. 108 (2012) 77–86. doi:10.1016/j.jfoodeng.2011.07.026.

[100] K.K. Latt, T. Kobayashi, Ultrasound-membrane hybrid processes for enhancement of filtration properties, Ultrason. Sonochem. 13 (2006) 321–328. doi:10.1016/j.ultsonch.2005.05.002.

[101] J. Li, R.D. Sanderson, E.P. Jacobs, Ultrasonic cleaning of nylon microfiltration membranes fouled by Kraft paper mill effluent, J. Memb. Sci. 205 (2002) 247–257. doi:10.1016/S0376-7388(02)00121-7.

[102] Y. Matsumoto, T. Miwa, S.I. Nakao, S. Kimura, Improvement of membrane permeation performance by ultrasonic microfiltration, J. Chem. Eng. Japan. 29 (1996) 561–567. doi:10.1252/jcej.29.561.

[103] T.M. Patel, K. Nath, Alleviation of flux decline in cross flow nanofiltration of two-component dye and salt mixture by low frequency ultrasonic irradiation, Desalination. 317 (2013) 132–141. doi:10.1016/j.desal.2013.03.001.

[104] D. Feng, J.S.J. van Deventer, C. Aldrich, Ultrasonic defouling of reverse osmosis membranes used to treat wastewater effluents, Sep. Purif. Technol. 50 (2006) 318–323. doi:10.1016/j.seppur.2005.12.005.

[105] Y.J. Choi, S.H. Kim, S. Jeong, T.M. Hwang, Application of ultrasound to mitigate calcium sulfate scaling and colloidal fouling, Desalination. 336 (2014) 153–159. doi:10.1016/j.desal.2013.10.011.

[106] H. Kim, Y. Lee, M. Elimelech, A. Adout, Y.C. Kim, Experimental study of ultrasonic effects on flux enhancement in forward osmosis process, in: Meet. Abstr. No. 4, The Electrochemical Society, 2012: pp. 90–90.

[107] J. Heikkinen, H. Kyllönen, E. Järvelä, A. Grönroos, C.Y. Tang, Ultrasound-assisted forward osmosis for mitigating internal concentration polarization, J. Memb. Sci. 528 (2017) 147–154. doi:10.1016/j.memsci.2017.01.035.

[108] B.S. Chanukya, N.K. Rastogi, Ultrasound assisted forward osmosis concentration of fruit juice and natural colorant, Ultrason. Sonochem. 34 (2017) 426–435. doi:10.1016/j.ultsonch.2016.06.020.

[109] D. Hou, Z. Wang, G. Li, H. Fan, J. Wang, H. Huang, Ultrasonic assisted direct contact membrane distillation hybrid process for membrane scaling mitigation, Desalination. 375 (2015) 33–39. doi:10.1016/j.desal.2015.07.018.

[110] D. Hou, G. Dai, H. Fan, H. Huang, J. Wang, An ultrasonic assisted direct contact membrane distillation hybrid process for desalination, J. Memb. Sci. 476 (2015) 59–67. doi:10.1016/j.memsci.2014.11.028.

[111] C. Zhu, G.L. Liu, C.S. Cheung, C.W. Leung, Z.C. Zhu, Ultrasonic stimulation on enhancement of air gap membrane distillation, J. Memb. Sci. 161 (1999) 85–93. doi:10.1016/S0376-7388(99)00105-2.

[112] D. Hou, L. Zhang, C. Zhao, H. Fan, J. Wang, H. Huang, Ultrasonic irradiation control of silica fouling during membrane distillation process, Desalination. 386 (2016) 48–57. doi:10.1016/j.desal.2016.02.032.

[113] P. Sui, X. Wen, X. Huang, Membrane fouling control by ultrasound in an anaerobic membrane bioreactor, Front. Environ. Sci. Eng. China. 1 (2007) 362–367. doi:10.1007/s11783-007-0062-9.

[114] P. Sui, X. Wen, X. Huang, Feasibility of employing ultrasound for on-line membrane fouling control in an anaerobic membrane bioreactor, Desalination. 219 (2008) 203–213. doi:10.1016/j.desal.2007.02.034.

[115] M. Xu, X. Wen, X. Huang, Z. Yu, M. Zhu, Mechanisms of membrane fouling controlled by online ultrasound in an anaerobic membrane bioreactor for digestion of waste activated sludge, J. Memb. Sci. 445 (2013) 119–126. doi:10.1016/j.memsci.2013.06.006.

[116] T. Kobayashi, T. Kobayashi, Y. Hosaka, N. Fujii, Ultrasound-enhanced membrane-cleaning processes applied water treatments: Influence of sonic frequency on filtration treatments, Ultrasonics. 41 (2003) 185–190. doi:10.1016/S0041-624X(02)00462-6.

[117] S. Muthukumaran, K. Yang, a. Seuren, S. Kentish, M. Ashokkumar, G.W. Stevens, all authored are required, The use of ultrasonic cleaning for ultrafiltration membranes in the dairy industry, Sep. Purif. Technol. 39 (2004) 99–107. doi:10.1016/j.seppur.2003.12.013.

[118] X. Chai, T. Kobayashi, N. Fujii, Ultrasound-associated cleaning of polymeric membranes for water treatment, Sep. Purif. Technol. 15 (1999) 139–146. doi:10.1016/S1383-5866(98)00091-4.

[119] A. Maskooki, S.A. Mortazavi, A. Maskooki, Cleaning of spiralwound ultrafiltration membranes using ultrasound and alkaline solution of EDTA, Desalination. 264 (2010) 63–69. doi:10.1016/j.desal.2010.07.005.

[120] L. Wang, Q. Wang, Y. Li, H. Lin, Ultrasound-assisted chemical cleaning of polyvinylidene fluoride membrane fouled by lactic acid fermentation broth, Desalination. 326 (2013) 103–108. doi:10.1016/j.desal.2013.06.010.

[121] R.S. Juang, K.H. Lin, Flux recovery in the ultrafiltration of suspended solutions with ultrasound, J. Memb. Sci. 243 (2004) 115–124. doi:10.1016/j.memsci.2004.06.013.

[122] W. Jin, W. Guo, X. Lü, P. Han, Y. Wang, Effect of the Ultrasound Generated by Flat Plate Transducer Cleaning on Polluted Polyvinylidenefluoride Hollow Fiber Ultrafiltration Membrane, Chinese J. Chem. Eng. 16 (2008) 801–804. doi:10.1016/S1004-9541(08)60159-7.

[123] S. Muthukumaran, S. Kentish, S. Lalchandani, M. Ashokkumar, R. Mawson, G.W. Stevens, et al., The optimisation of ultrasonic cleaning procedures for dairy fouled ultrafiltration membranes, Ultrason. Sonochem. 12 (2005) 29–35. doi:10.1016/j.ultsonch.2004.05.007.

[124] M.J. Luján-Facundo, J. a. Mendoza-Roca, B. Cuartas-Uribe, S. Álvarez-Blanco, Ultrasonic cleaning of ultrafiltration membranes fouled with BSA solution, Sep. Purif. Technol. 120 (2013) 275–281. doi:10.1016/j.seppur.2013.10.018.

[125] J.Y. Lu, X. Du, G. Lipscomb, Cleaning membranes with focused ultrasound beams for drinking water treatment, Proc. - IEEE Ultrason. Symp. (2009) 1195–1198. doi:10.1109/ULTSYM.2009.5441719.

[126] E. Alventosa-Delara, S. Barredo-Damas, M.I. Alcaina-Miranda, M.I. Iborra-Clar, Study and optimization of the ultrasound-enhanced cleaning of an ultrafiltration ceramic membrane through a combined experimental-statistical approach, Ultrason. Sonochem. 21 (2014) 1222–1234. doi:10.1016/j.ultsonch.2013.10.022.

[127] M.-W. Wan, H.-L. Yang, C.-H. Chang, F. Reguyal, C.-C. Kan, Fouling Elimination of PTFE Membrane under Precoagulation Process Combined with Ultrasound Irradiation, J. Environ. Eng. 138 (2012) 337–343. doi:10.1061/(ASCE)EE.1943-7870.0000406.

[128] C.C. Kan, D.A.D. Genuino, K.K.P. Rivera, M.D.G. de Luna, Ultrasonic cleaning of polytetrafluoroethylene membrane fouled by natural organic matter, J. Memb. Sci. 497 (2016) 450–457. doi:10.1016/j.memsci.2015.08.031.

[129] A. Maskooki, T. Kobayashi, S.A. Mortazavi, A. Maskooki, Effect of low frequencies and mixed wave of ultrasound and EDTA on flux recovery and cleaning of microfiltration membranes, Sep. Purif. Technol. 59 (2008) 67–73. doi:10.1016/j.seppur.2007.05.028.

[130] J. Wang, X. Gao, Y. Xu, Q. Wang, Y. Zhang, X. Wang, all authored are required, Ultrasonic-assisted acid cleaning of nanofiltration membranes fouled by inorganic scales in arsenic-rich brackish water, Desalination. 377 (2016) 172–177. doi:10.1016/j.desal.2015.09.021.

[131] L. A. Koh, H.H Nguyen, J. Chandrapala, B. Zisu, M. Ashokkumar, S. E. Kentish, The use of ultrasonic feed pre-treatment to reduce membrane fouling in whey ultrafiltration, J Membr. Sci. 453 (2014) 230–239. doi:10.1016/j.memsci.2013.11.006.

[132] R.A. Al-juboori, "Ultrasound technology as a pre-treatment for biofouling control in Reverse Osmosis (RO) system," University of Southern Queenland, Australia, 2012.

[133] D. H. Oyib, "Ultrasound Technology in Water Treatment: Suppressing Algal Growth and Biofilm Formation," WaterWorld, 2009. [Online]. Available: http://www.waterworld.com/articles/2009/05/ultrasound-technology-in-water-treatment-suppressing-algal-growth-and-biofilm-formation.html. [Accessed 2 February 2018].

[134] E. Joyce, S.S. Phull, J.P. Lorimer, T.J. Mason, The development and evaluation of ultrasound for the treatment of bacterial suspensions. A study of frequency, power and sonication time on cultured Bacillus species, Ultrason. Sonochem. 10 (2003) 315–318. doi:10.1016/S1350-4177(03)00101-9.

[135] S.S. Phull , A.P. Newman, J.P. Lorimer, B. Pollet, T.J. Mason , The development and evaluation of ultrasound in the biocidal treatment of water, Ultrason. Sonochem. 4 (1997) 157–164. doi:10.1016/S1350-4177(97)00029-1.

[136] S. Broekman, O. Pohlmann, E.S. Beardwood, E. Cordemans de Meulenaer, Ultrasonic treatment for microbiological control of water systems, Ultrason. Sonochem. 17 (2010) 1041–1048. doi:10.1016/j.ultsonch.2009.11.011.

[137] S. Kertész, I. Kovács, C. Hodúr, G. Keszthelyi-Szabó, Ultrasound membrane hybrid processes for dairy wastewater treatment: pilot-scale analysis, Desalin. Water Treat. 57 (2016) 1-8. doi:10.1080/19443994.2016.1173386.

[138] I. Masselin, X. Chasseray, L. Durand-Bourlier, J.M. Lainé, P.Y. Syzaret, D. Lemordant, Effect of sonication on polymeric membranes, J. Memb. Sci. 181 (2001) 213–220. doi:10.1016/S0376-7388(00)00534-2.

[139] X. Wang, X. Li, X. Fu, R. Chen, B. Gao, Effect of ultrasound irradiation on polymeric microfiltration membranes, Desalination. 175 (2005) 187–196. doi:10.1016/j.desal.2004.08.044.